Coherent multi-level network oscillations create neural filters to favor quiescence over navigation in *Drosophila*

Davide Raccuglia[1,*,#], Raquel Suárez-Grimalt[1,2,*], Laura Krumm[2,4], Cedric B Brodersen[1], Anatoli Ender[1], Sridhar R. Jagannathan[1], York Winter[2,5], Genevieve Yvon-Durocher[1,2,+], Richard Kempter[2,4,6], Jörg RP Geiger[1,2], and David Owald[1,2,3,#]

[1]Institute of Neurophysiology, Charité – Universitätsmedizin Berlin, corporate member of Freie Universität Berlin, Humboldt-Universität zu Berlin and Berlin Institute of Health, Charitéplatz 1, 10117 Berlin, Germany

[2]Einstein Center for Neurosciences Berlin, Charitéplatz 1, 10117 Berlin, Germany

[3]NeuroCure, Charité – Universitätsmedizin Berlin, corporate member of Freie Universität Berlin, Humboldt-Universität zu Berlin and Berlin Institute of Health, Charitéplatz 1, 10117 Berlin, Germany

[4] Institute for Theoretical Biology, Department of Biology, Humboldt-Universität zu Berlin, Philippstr. 13, 10115 Berlin, Germany

[5] Institute of Biology, Department of Biology, Humboldt-Universität zu Berlin, Philippstr. 13, 10115 Berlin, Germany

[6] Bernstein Center for Computational Neuroscience Berlin, Philippstr. 13, 10115 Berlin, Germany

+ = present address: Biomedical Sciences Building, University of Bristol, Tankard's Cl, University Walk, Bristol, BS8 1TD

* = shared first authors

= correspondence to DR (davide.raccuglia@charite.de) and DO (david.owald@charite.de)

Abstract

For all animals, undisturbed periods of rest are essential for undergoing recuperative processes. How neural interactions create brain states capable of dissociating an animal from its external world to promote quiescence remains a fundamental question. Here, we show how coherent network oscillations can create neural filters that favor a quiescent brain state over a state that promotes navigation. Circadian regulation and excitability of the *Drosophila* sleep homeostat (dFSB) generate nighttime specific slow-wave coherence between neural networks mediating sleep need (R5) and networks gating locomotion (helicon cells). Optogenetically mimicking coherent activity reveals that temporally fine-tuned R5 oscillations promote a quiescent state and reduce responsiveness to visual stimuli by hierarchically overruling locomotion-promoting helicon cells. We uncover that R5 and helicon bidirectionally regulate behavioral responsiveness by providing antagonistic inputs to head direction targets (EPG). Thus, coherent oscillations can form the mechanistic basis of neural filters by temporally associating antagonistic inputs and therefore reducing the functional connectivity between locomotion gating and navigational networks.

Introduction

Whether we execute cue-driven behavior or remain unresponsive depends on the neural integration of internal states and the salience of sensory stimuli. External information is thought to be processed through efficient neural filtering mechanisms, which largely differ during wake and sleep, thereby defining gateways to the whole brain. Filters regulate the neural representation of sensory information and therefore create a switch that determines whether we enter an 'allocentric' mode directed to external stimuli or remain in an 'egocentric', internal-centered setting (Lu et al., 2022; Lyu et al., 2022). In mammals the thalamus has been implicated as a filter for sensory information, relaying it to higher order cortical networks (Andrillon and Kouider, 2020; Crunelli and Hughes, 2010; Gent et al., 2018). The lowest degree of behavioral responsiveness occurs during deep sleep, during which thalamo-cortical interactions generate slow-wave activity (SWA) that result from electrical coherence across cortical networks (Buzsaki and Draguhn, 2004). It is therefore conceivable that oscillatory activity patterns could be suited for providing a certain 'cut-off' while retaining the flexibility for transduction of salient or strong stimuli. Experimental evidence and knowledge on the mechanistic underpinnings however remain limited. Strikingly, SWA associated with sleep and sleep need has been observed in mammals (Siclari and Tononi, 2017), birds (Low et al., 2008), reptiles (Shein-Idelson et al., 2016), fish (Leung et al., 2019), crabs (Ramon et al., 2004) and recently in the vinegar fly *Drosophila melanogaster* (Raccuglia et al., 2019), and could represent an evolutionarily optimized mechanism for constructing neural filters. Indeed, mounting evidence suggests that neural coherence generating SWA is a network-autonomous marker of sleep need which might represent a fundamental neural principle for suppressing sensory processing to promote the reorganization of synaptic connectivity (Krueger et al., 2019; Suárez-Grimalt and Raccuglia, 2021; Vyazovskiy et al., 2011). However, how oscillatory coherence maintains quiescent states, gates signals to the brain and regulates behavioral responsiveness on a mechanistic network level remains largely unclear.

In *Drosophila*, behavioral responsiveness is particularly reduced during quiescent states, which are defined by prolonged inactivity (≥ 5 min) (Shaw et al., 2000). These quiescent states meet the criteria for sleep as they underlie homeostatic regulation (Shaw et al., 2000). Interestingly, transitions from an active state to a quiescent state are accompanied by an

increase of oscillatory activity in the central brain (Yap et al., 2017). Recent years have established that sensory processing, behavioral responsiveness and sleep in *Drosophila* are integrated by a higher sensory processing center called the central complex (Donlea, 2019).

Importantly, in *Drosophila*, the individual circuit elements of the central complex are known and therefore allow a targeted analysis of network activity and its mechanistic relationship to quiescent states. While the network comprising the fan-shaped body (dFSB) functions as a homeostatic sleep switch (Donlea et al., 2009; Kempf et al., 2019; Pimentel et al., 2016), ExR1/helicon cells are part of a network which processes visual information and gates locomotion (Donlea et al., 2018). The R5 network, based on its connectivity likely engages in both navigation and sleep regulation (Blum et al., 2021; Flores-Valle et al., 2021; Huang et al., 2020; Liu et al., 2016; Raccuglia et al., 2019; Vafidis et al., 2022). Indeed, we recently discovered that in the R5 circuit, network-specific synchronization generating compound SWA arises over the day to integrate circadian and homeostatic sleep drive, promoting consolidated sleep phases to ensure adequate sleep quality (Raccuglia et al., 2019).

In this study, we directly target circuit elements of the central complex to investigate how the functional components of reciprocally connected networks (dFSB-helicon-R5) interact to create a filtering mechanism that maintains quiescence. Using a strategy that combines genetically-encoded voltage and Ca^{2+} sensors with optogenetics, we discovered that within this circuitry circadian and homeostatic sleep regulation are integrated to generate a brain state that is characterized by coherent SWA. Particularly, the locomotor-promoting helicon and sleep need mediating R5 circuit elements synchronize their electrical patterns during the night. Optogenetically mimicking these activity patterns during the day induced a quiescent state with reduced behavioral responsiveness to light. We further show that head direction neurons (EPG), which are part of a navigational system, receive antagonistic input from helicon and R5 to bidirectionally regulate behavioral responsiveness. We therefore propose that oscillatory network coherence provides the mechanistic basis for a neural filter by rhythmically associating antagonistic inputs, effectively reducing the functional connectivity between locomotion gating networks and the navigational system.

105 ## Results

106 **Electrical slow-wave activity in the master sleep homeostat in *Drosophila***

107 In humans, sleep depth and mounting tiredness are associated with SWA (0.5-4 Hz) spreading
108 across several brain regions (Adamantidis et al., 2019). We recently identified that the
109 emergence of SWA in the R5 network of *Drosophila* is correlated to undisrupted sleep and
110 reduced behavioral responsiveness (Raccuglia et al., 2019). Similar to thalamo-cortical circuits,
111 the current *in vivo* brain state and the ability to generate SWA is maintained in the intact
112 explant brain (Liu et al., 2016; Raccuglia et al., 2019; Sanchez-Vives and McCormick, 2000),
113 enabling us to study activity patterns and network interactions characteristic for specific brain
114 states. We therefore used this approach to investigate whether sleep-relevant SWA was a
115 local phenomenon constrained to R5 neurons or also becomes manifest within other
116 networks.

117

118 We first focused on the dFSB network which comprises neurons that integrate and execute
119 sleep drive (Donlea et al., 2014). To directly test whether compound electrical activity is
120 correlated between the dFSB and R5 network we performed dual color voltage imaging
121 experiments by simultaneously expressing the green voltage indicator (GEVI) ArcLight (Cao et
122 al., 2013; Raccuglia et al., 2016) and the red voltage indicator Varnam (Kannan et al., 2018) in
123 R5 and dFSB, respectively (**Fig. 1A-C**). We focused on presynaptic compound activity because
124 it represents the neural activity of the entire networks. We found that the presynaptic
125 compound activity of R5 and the dFSB were largely synchronized at night (**Fig. 1D**). To verify
126 interactions between these structures, we investigated whether diurnal variations of the
127 electrical patterns observed in R5 were also observable in the dFSB. Indeed, compared to the
128 morning we observed an increase in slow-wave power (0.5-1.5 Hz) at night when measuring
129 the presynaptic compound signal, which represents the coherent activity of the whole dFSB
130 network (**Fig. 1E, F**). Independent multi-cellular recordings revealed low overall activity of
131 dFSB neurons in the morning hours (**Fig. S1A**). General activity markedly increased in the
132 evening (**Fig. 1G**) and power analysis revealed an activity peak between 0.5-1 Hz (**Fig. 1H**).
133 However, unlike what we previously observed for the R5 network (Raccuglia et al., 2019),
134 activity was only loosely correlated between the single units regardless of whether measured
135 during the morning or the night hours (**Fig. S1B**), indicating that changes in single-cell
136 excitability are sufficient to drive diurnal changes at the network level.

137 We conclude that both dFSB and R5 networks exhibit diurnal variations in oscillatory activity
138 and are likely functionally interconnected, as previously reported R5 to dFSB interactions with
139 respect to mediating sleep drive would suggest (Liu et al., 2016).
140
141 **Reciprocal functional interactions between neural circuits promoting sleep**
142 To test for functional interactions of network activity patterns, we first asked whether R5
143 activation could induce dFSB oscillations (**Fig. 2A-C**). We suppressed spontaneous network
144 activity using a previously established high Mg^{2+} extracellular saline (Raccuglia et al., 2019)
145 and optogenetically stimulated R5 neurons using genetic targeting of the red-light shifted
146 channelrhodopsin CsChrimson (Klapoetke et al., 2014) while monitoring intracellular Ca^{2+} in
147 presynaptic terminals of the dFSB (**Fig. 2A**). As presynaptic Ca^{2+} is an adequate proxy for
148 synaptic output, we here focused on compound Ca^{2+} oscillations of the sleep drive-mediating
149 neural circuits. Optogenetic stimulation of R5 reliably induced or amplified dFSB presynaptic
150 SWA between 0-1 Hz (**Fig. 2B, Fig. S2A, B**). This effect was statistically significant only after
151 terminating optogenetic activation (**Fig. 2C**), indicating that activation of R5 neurons can lead
152 to longer lasting physiological changes in the dFSB. This finding is in accordance with the
153 observation that sleep need increases mainly after thermogenetic activation of R5 and
154 moreover requires synaptic output from the dFSB (Liu et al., 2016). Interestingly, the power
155 of the observed SWA in dFSB neurons was more pronounced during the subjective night (**Fig.
156 2C**), demonstrating the influence of the circadian clock on interactions between sleep drive
157 mediating neural circuits.
158 Next, we optogenetically activated the dFSB and recorded presynaptic Ca^{2+} activity in R5 (**Fig.
159 2D**). Optogenetic activation of the dFSB did not elicit Ca^{2+} oscillations during the day (**Fig. 2E**)
160 but elicited pronounced oscillations between 0.5-1.5 Hz during stimulation at nighttime (**Fig.
161 2F** and **Fig. S2C, D**). Moreover, in some cases, R5 SWA persisted even after optogenetic
162 activation ceased (**Fig. S2E**), suggesting that increased excitability of the dFSB at night can
163 entrain R5 oscillations and might thus affect sleep need on a larger time scale.
164 To directly test whether the increased excitability of the dFSB at night drives SWA in R5, we
165 optogenetically hyperpolarized the dFSB using the light-gated chloride channel GtACR
166 (Mohammad et al., 2017) (**Fig. 2G**). To access the potential effect of inhibition, we used a low
167 Mg^{2+} extracellular saline that does not suppress spontaneous activity (Raccuglia et al., 2019).
168 Indeed, activating GtACR in the dFSB reduced oscillatory power of the R5 network (**Fig. 2H, I**),

169 further supporting the notion that sleep need mediating SWA in R5 neurons is facilitated by
170 increased excitability within the sleep-executing neurons of the dFSB. This effect was not
171 observable in controls not expressing GtACR (**Fig. 2H, I**). However, often R5 SWA partially
172 recovered after the start of optogenetic inhibition (**Fig. S2F, G**), suggesting that R5 SWA is
173 stabilized either through other synaptic inputs (such as TuBu) (Lamaze et al., 2018; Raccuglia
174 et al., 2019) or through cell-autonomous promotion of SWA.
175 Our data so far suggest that functional interactions between network activity in the dFSB and
176 R5 generate sleep drive mediating-SWA dependent on the time of the day. Oscillatory
177 frequencies observed after activating specific networks slightly vary from spontaneously
178 occurring SWA at night, suggesting that compound SWA in the *Drosophila* brain is fine-tuned
179 by an interplay of several networks. After demonstrating that prominent sleep-regulating
180 structures exhibit similar, but not identical mutually interactive oscillations at night, we next
181 addressed to what extent the temporal structure of network activity was relevant for
182 behavior.
183
184 **Neural circuits mediating sleep drive acutely control locomotion, postural control and**
185 **behavioral programs associated with quiescence**
186 Activation of both R5 and dFSB has been shown to have profound impact on fly sleep behavior
187 (Liu et al., 2016; Pimentel et al., 2016; Raccuglia et al., 2019). We now tested how the temporal
188 architecture of electrical patterns that are characteristic of the "sleepy" brain state at night
189 affects behavioral activity during the day.
190 We devised a paradigm for tracking freely moving flies in a small circular arena while
191 performing temporally fine-tuned optogenetic activation experiments (**Fig. 3A**). To
192 demonstrate that the locomotion of flies in this arena is subject to their internal sleep need,
193 we compared locomotor activity of rested and sleep deprived flies (**Fig. 3B**). As expected, the
194 mean velocity of sleep deprived flies was significantly reduced compared to rested flies (**Fig.**
195 **3B**). Moreover, about 56% of sleep deprived flies were immobile for 5 min, which represents
196 the generally accepted criteria for sleep (Shaw et al., 2000), demonstrating that the flies'
197 locomotor activity in the arena is indeed subject to their internal sleep need.
198 We first asked whether 1 Hz optogenetic activation of the dFSB could acutely regulate
199 locomotor activity (**Fig. 3C**). Importantly, optogenetic activation of dFSB neurons at 1 Hz had
200 previously been shown to reliably promote the naturally occurring oscillatory pattern in single

201 dFSB neurons (Troup et al., 2018). To be more sensitive to the induction of potential sleep
202 states, we performed these experiments during the subjective day (ZT 1-10). 1 Hz stimulation
203 of the dFSB decreased the walking velocity as well as the time spent walking (**Fig. 3D-E** and
204 **S3A**), which is in accordance with the strongly sleep-promoting function of the dFSB. To
205 exclude the possibility that the observed behavior was a visually triggered response to pulsed
206 light, we evaluated the effect of the optogenetic protocol on the locomotion of flies carrying
207 only the UAS-CsChrimson transgene. We found that pulsed light slightly reduced locomotor
208 activity (**Fig. 3E, S3A**, compare to **3G**). However, inhibition of locomotor activity through dFSB
209 activation was considerably stronger (**Fig. 3E** and **S3A**). To test whether inhibition of
210 locomotion was frequency-specific, we next stimulated dFSB neurons at 10 Hz. We observed
211 locomotor phenotypes comparable to 1 Hz stimulation, indicating that the activation
212 frequency and correlating increase in stimulation intensity was not crucial to increase sleep
213 need (**Fig. S3B**).
214 We next tested whether acute rhythmic optogenetic activation of R5 would similarly affect
215 locomotion (**Fig. 3F**). Indeed, activating R5 at 1 Hz significantly reduced locomotion similar to
216 what we observed when stimulating the dFSB (**Fig. 3G, H, S3C**). During optogenetic stimulation
217 of R5, flies displayed short walking bouts as well as frequent grooming (**Fig. S3F**). Unlike what
218 was observed when stimulating the dFSB, locomotion recovered much slower after
219 stimulation offset, not reverting to normal for the following 5 min (**Fig. 3G, H**). This is in line
220 with R5 activity entraining the involved neural circuits to prepare flies for sleep and promote
221 more consolidated sleep phases (Raccuglia et al., 2019). To determine whether flies still
222 showed appropriate locomotor behavior during optogenetic stimulation of R5, we
223 investigated whether flies were capable of reaching higher velocities while walking ("walking
224 velocity") by only considering movements > 0.25 cm/s (see **Methods**, **Fig. S3C**). We found that
225 this walking velocity was only slightly affected (**Fig. S3C**), indicating that reduced locomotion
226 was mainly due to a reduction in time spent walking**.** Moreover, we also examined the flies'
227 behavioral responsiveness to an air-puff during 1 Hz R5 stimulation and found that flies
228 reacted to this strong stimulus by increasing their walking velocity (**Fig. S3D**). These findings
229 suggest that R5 activation at 1 Hz reduces locomotor activity while leaving the ability to walk
230 and respond to strong stimuli intact. We therefore conclude that 1 Hz R5 activation induces a
231 quiescent state characterized by reduced locomotor activity and frequent grooming, which in
232 fact has been associated with periods of rest that occur prior to sleep (Qiao et al., 2018).

233 We next explored whether the behavioral outcome following R5 activation was frequency-
234 specific. Unlike the effects observed when stimulating at 1Hz, 10 Hz protocols rendered flies
235 immobile and ~90% of flies lost postural control during optogenetic activation, sometimes
236 lasting for 5 min post-stimulation (**Fig. 3I, S3E-G**). Stimulating R5 neurons at 0.1 Hz did not lead
237 to a measurable impact on the flies' behavior (**Fig. S3E**). Therefore, contrary to the dFSB, the
238 activation frequency and intensity mattered for the R5 network (**Fig. 3I and S3E**), potentially
239 placing the R5 network as instructive for an ongoing brain state (such as sleep). While the slow
240 oscillations observed in R5 allows the flies to maintain natural body posture during
241 quiescence, it is possible that over-stimulating R5 neurons at 10 Hz overrules downstream
242 effectors involved in standing upright. In line with this, 1 Hz optogenetic activation of R5 in
243 rested flies reduced locomotor activity to the level of awake sleep deprived flies (**Fig. 3J**),
244 indeed suggesting that 1 Hz R5 activation is specific to increasing sleep need in awake animals.
245 Taken together, these data indicate that acute activation of neural circuits mediating sleep
246 drive at a frequency band of sleep-relevant SWA induces a quiescent state characterized by
247 reduced locomotion.
248
249 **Sleep-promoting R5 neurons and locomotion-gating helicon cells synchronize electrical**
250 **patterns at night**
251 Our data demonstrate reciprocal functional interactions between the dFSB and R5
252 networks and also indicate that these structures can act as functional analogs at the
253 behavioral level. Using the recently published hemiconnectome of *Drosophila* (Scheffer et al.,
254 2020), we next investigated putative neural connections between the dFSB and R5
255 and found no direct synaptic connections (**Fig. 4A, B**). Instead, our analysis revealed that R5
256 neurons are highly interconnected with the previously identified helicon network (Donlea et
257 al., 2018). These four neurons make reciprocal all-to-all synaptic connections with R5 (**Fig.**
258 **S4A**) that represent about 24% of R5 input and output connections (**Fig. 4A**). Similarly, R5
259 neurons are one of the main pre- and postsynaptic partners of helicon cells (**Fig. S4B**).
260 Consistent with previous observations showing that dFSB neurons inhibit visually evoked
261 responses in helicon cells (Donlea et al., 2018), we found that helicon cells are reciprocally
262 connected to the dFSB (**Fig. S4C**) (Hulse et al., 2021). Our analysis further indicates that, as
263 previously suggested (Donlea et al., 2018), recurrent connections from helicon cells could

264 constitute a main route to relay neural information between the dFSB and R5 networks and
265 vice versa (**Fig. 4B and S4D**).
266 Since helicon cells and R5 neurons seem to play a role in both visually guided navigation and
267 mediating sleep need (Flores-Valle et al., 2021; Seelig and Jayaraman, 2013), it is likely that
268 temporal interactions between the activity patterns of these circuits regulate locomotor
269 activity during wake and sleep. To first probe for electrical network activity in helicon cells at
270 night, we expressed the voltage indicator ArcLight (**Fig. S4E**) and found spontaneous
271 compound activity between 0.5-1.5 Hz (**Fig. S4F, G**), indicating similarities to R5 oscillatory
272 activity.
273 To investigate a direct relationship between R5 and helicon electrical patterns, we
274 simultaneously recorded the electrical compound activity at their overlapping presynaptic
275 sites by performing dual color voltage imaging experiments expressing the green voltage
276 indicator ArcLight in R5 and the red voltage indicator Varnam in helicon (**Fig. 4C**). We
277 confirmed that in both R5 and helicon oscillatory power (0.5-1.5 Hz) is increased at night
278 compared to the subjective morning (**Fig. 4D, E**). Most interestingly, correlation between the
279 electrical patterns of these neural populations was significantly increased at night (**Fig. 4F**). To
280 control for different kinetics of the voltage indicators, we swapped the expression (expressing
281 ArcLight in helicon cells and Varnam in R5 neurons) and observed similarly high correlation at
282 nighttime (**Fig. S4H-J**). Therefore, our data suggest that helicon compound activity might be
283 entrained by R5 slow-wave activity.
284
285 **Modelling predicts that R5 entrains helicon oscillation via excitatory connections**
286 Based on our physiological findings, we next turned to theoretical modeling to further
287 investigate how network interactions could steer behavior. Our data suggests that R5 could
288 function as the master oscillator, entraining synchronous oscillatory activity in helicon. We
289 used the Izhikevich model to simulate synchronization of single R5 neurons (please see
290 **Supplemental text** and **Fig. S5-1** legend for detailed information). R5 neurons are highly
291 interconnected (**Fig. S5-1A**), which could allow them to synchronize through mutual
292 interaction. R5 neurons, however, have been identified to be GABAergic (Hanesch et al.,
293 1989), a finding we confirmed using immunofluorescence (**Fig. S5-1C**). Not surprisingly, as
294 inhibitory pulse-coupled oscillators are known to usually stay out of sync (Terman et al., 1998),
295 we found that in order to simulate synchronization patterns similar to those experimentally

296 observed, we required mixed excitatory and inhibitory output of R5 neurons (**Fig. S5-1E**). In
297 the model, we varied the relative strength of the mixed inhibitory and excitatory synaptic
298 coupling among R5 neurons and observed that synchronization correlated with the relative
299 strength of excitation compared to inhibition within the network (**Fig. S5-1E-H**). The main
300 excitatory neurotransmitter in insect brains is acetylcholine (Fayyazuddin et al., 2006). To
301 experimentally verify whether R5 also had excitatory outputs, we used an endogenously HA-
302 tagged vesicular acetylcholine transporter (VAChT), a bona fide marker for cholinergic vesicles,
303 that can be induced to label cholinergic output sites in specific neural populations (Pankova
304 and Borst, 2017). Strikingly we identified several cholinergic R5 sites (**Fig. S5-1B**), supporting
305 a R5 network with mixed inhibitory and excitatory output as source for the observed
306 oscillations. We next added helicon cells to our model to investigate coherent activity of
307 helicon and R5 networks throughout the day. Helicon, as a purely excitatory network
308 recurrently connected to R5, was modeled to switch from a more polarized and active state
309 in the morning ('upstate') to a more hyperpolarized, inactive state ('downstate') at nighttime
310 (**Fig. 5A**). This was warranted, as dFSB stimulation had previously been shown to hyperpolarize
311 helicon (Donlea et al., 2018). Moreover, providing further experimental data for our model,
312 we found through baseline fluorescence quantification of the voltage indicator ArcLight, that
313 single helicon cells were more hyperpolarized in the evening compared to the morning hours
314 (**Fig. S5-1D**). Therefore, our simulation is in line with the dFSB paving the path for R5-mediated
315 association of helicon activity at night (compare **Fig. 2**) by rendering helicon less responsive to
316 inhibitory (while still responsive to excitatory) input from R5 when helicon's resting membrane
317 potential is closer to the chloride reversal potential (Barker and Harrison, 1988). Indeed, our
318 simulation resulted in 1 Hz oscillations at night for both helicon and R5, while helicon was not
319 oscillating in the daytime settings (**Fig. 5B**). Moreover, reminiscent of our experimental
320 findings (**Fig. 4F**), both networks were highly synchronized at night and R5 activity slightly
321 preceded helicon activity, suggesting that R5 drives compound oscillations in helicon cells (**Fig.
322 5C**). Given the close match between our simulation and experimental findings, we used our
323 model to predict the outcome of experiments performing artificial stimulations. To do so, we
324 simulated network activity when stimulating either network or both together (**Fig. 5D**).
325 Strikingly, we found that the underlying network activity architecture showed dominant R5
326 activity over helicon (**Fig. 5E**), suggesting that activation of R5 and helicon at the same time
327 should have a similar behavioral outcome as activating R5 on its own (please see supplemental

328 information for more details). Indeed, simultaneous activation closely resembles the observed
329 nighttime configuration (**Fig. 5B**). We turned back to behavioral experiments to test this
330 prediction.
331
332 **Network coherence regulates behavioral responsiveness**
333 In mammals, synchronization of SWA between and within neural circuits occurs during deep
334 sleep and local sleep in awake individuals and is hypothesized to establish neural filters that
335 suppresses behavioral responsiveness to external stimuli (Quercia et al., 2018). To investigate
336 whether synchronization between R5 and helicon play a role in regulating behavioral
337 responsiveness during sleep, we used optogenetics to separately and simultaneously activate
338 these networks at 1 Hz in sleeping flies (**Fig. 5F-H**). After sleep deprivation, sleeping flies were
339 exposed to green light to arouse them and elicit visually evoked locomotion while
340 simultaneously applying red light pulses at 1 Hz for network-specific optogenetic stimulation
341 (**Fig. 5F**). As shown for rested control flies (compare **Fig. 3G**), all genotypes showed slight
342 arousal to red light (**Fig. 5G, and S5-2A, B**). However, as expected, helicon cell stimulation led
343 to the strongest degree of arousal (**Fig. S5-2A**) with most flies being awakened (**Fig. S5-2B**),
344 while arousal during R5 stimulation was consistent with the control (**Fig. S5I**). During
345 stimulation with green light, control flies and helicon activation showed the highest degree of
346 visually induced locomotion (**Fig. 5G-H**). In contrast, visually triggered locomotion was not
347 observed during stimulation of R5 neurons. While flies were capable of reacting to a strong
348 air-puff (**Fig. S3D**), optogenetically induced R5 oscillations seem to establish a neural filter that
349 blocks visually induced locomotion. Interestingly, compared to R5 activation alone,
350 synchronous activation of R5 and helicon led to a stronger reduction of locomotor activity (**Fig.**
351 **5H**) and only a small fraction of flies were awakened by green light (**Fig S5-2B**), indicating that
352 R5 and helicon synchronization might establish a more efficient neural filter. Together, these
353 findings indicate that sleep drive mediated by R5 oscillations overrides gating of locomotion
354 by helicon cells and further demonstrates that synchronization between these networks locks
355 the locomotion-initiating networks into a state that, dependent on sleep need, reduces
356 sensory processing and behavioral responsiveness. Of note, in the model, R5 and helicon
357 activation led to a slightly larger 1 Hz oscillation of the R5 network than the activation of R5
358 alone (**Fig. 5E**). Similarly, a 1 Hz activation of only helicon cells had a relatively small impact on

359 inducing oscillations in R5 (**Fig. 5E**), which matches the behavioral observation that helicon
360 cell stimulation induced arousal and not quiescence (**Fig. 5G** and **Fig. S5-2A**).
361
362 **Helicon and R5 antagonistically regulate locomotor activity and behavioral responsiveness**
363 **via modulation of head direction neurons**
364 We next aimed at investigating the mechanistic basis of how R5 and helicon synchronization
365 could regulate behavioral responsiveness. We therefore turned back to the connectome and
366 found that helicon cells as well as R5 neurons are connected to EPG neurons (**Fig. 6A**), which
367 are head-direction neurons representing the fly's heading direction and initiating body turns
368 towards or away from sensory stimuli (Green et al., 2017; Hulse et al., 2021; Kim et al., 2017;
369 Turner-Evans et al., 2017; Vafidis et al., 2022). In fact, we found that for about 70% of R5-to-
370 EPG synaptic connections the nearest non-R5 neighbor were helicon-to-EPG synapses (**Fig. 6A,**
371 **B**). Moreover, within the inner parts of the ring, where there are no R5 synapses, helicon-EPG
372 synapses can be found in close proximity to synaptic input of sleep-regulating R3 neurons
373 (Aleman et al., 2021; Hulse et al., 2021) (**Fig. 6B**), indicating that these synaptic motifs and
374 their spatial relations could be major sites of integrating navigation and sleep regulation
375 (Flores-Valle et al., 2021).
376 To test whether activity in the head-direction system is, similar to R5 and helicon, subject to
377 diurnal variation we used ArcLight to record the EPG compound electrical activity (**Fig. 6C-E**).
378 In the morning, EPG neurons displayed non-oscillatory events comprised of de- and
379 hyperpolarizations (**Fig. 6D**). Depolarizations occurred at an average rate of 1.2 every 10 s in
380 the morning and significantly dropped at night (**Fig. 6E**).
381 By expressing CsChrimson in R5 or helicon we next tested whether these networks could be
382 responsible for regulating activity in the EPG network (**Fig. 6F**). In fact, we found that R5
383 hyperpolarizes EPG neurons, while activation of helicon cells led to strong depolarizations (**Fig.**
384 **6G, H**), indicating that R5 and helicon cells modulate EPG activity via antagonistic
385 neurotransmitter inputs.
386 Our data therefore predict that de- and hyperpolarizing EPG neurons would have opposing
387 effects on locomotor activity and behavioral responsiveness. We tested this by directly de-
388 and hyperpolarizing EPG in rested flies using CsChrimson and GtACR respectively (**Fig. 6I-N**).
389 While depolarizing EPG neurons at 1 Hz had no effect on locomotion (**Fig. S6A**), activating EPG
390 neurons at higher frequencies (10 Hz) increased locomotor activity particularly at the

391 beginning of the stimulation (**Fig. 6J**). Moreover, flies displayed increased turning behavior
392 throughout the stimulation (**Fig. 6K**). Interestingly, immediately after ceasing EPG activation
393 flies transitioned to a quiescent state with starkly reduced locomotion (**Fig. 6J**), which suggests
394 homeostatic regulation of locomotor activity through EPG neurons.
395 We next tested whether GtACR-mediated hyperpolarization of EPG can actually reduce
396 locomotor activity (**Fig. 6L**). In control flies, constant green light leads to a sudden increase in
397 locomotor activity (**Fig. 6M, N**), demonstrating the behavioral responsiveness to visual stimuli.
398 When we simultaneously inhibited EPG, flies did not respond to green light but rather
399 completely stopped moving and about 45% of flies lost postural control (**Fig. 6M, N and S6D,**
400 **E**). This behavioral outcome is reminiscent of R5 activation (**Fig. 3 and 5**), indicating that
401 inhibition of EPG activity mediated through R5 can be a crucial component for fine-tuning
402 navigation during the day as well as modulating behavioral responsiveness and sleep depth
403 during the night. Together, our data is consistent with a mechanism, where R5 overrules input
404 of helicon to EPG at night by temporally associating helicon activity and thus creating a neural
405 filter to promote quiescence.
406
407
408 ## Discussion
409
410 The occurrence of brain-wide SWA during deep sleep (Adamantidis et al., 2019; Buzsaki and
411 Draguhn, 2004) as well as network-specific SWA during local sleep in awake individuals (Hung
412 et al., 2013; Quercia et al., 2018) suggests that coherent SWA could represent a neural filtering
413 mechanism that regulates sensory processing and behavioral responsiveness. How coherent
414 network activity suppresses behavioral responsiveness to promote a quiescent egocentric
415 state remains unclear to this day. Here, we discover a mechanism in *Drosophila*, where neural
416 networks promoting sleep need generate coherent oscillations across neural networks in
417 order to reduce the functional connectivity between locomotion gating networks and the
418 navigational system.
419
420 In this study, we demonstrate, to our knowledge for the first time, that SWA can provide the
421 temporal architecture that creates a “breakable” neural filter by providing an inhibitory tone
422 that suppresses gating of locomotion and at the same time maintains postural control to be
423 able to quickly respond to strong or salient stimuli (**Fig. 7**). Moreover, we reveal that network

interactions can form the mechanistic basis of filtering functions by temporally associating antagonistic neurotransmitter inputs to impede behavioral responses to external stimuli (**Fig. 7**).

Generating SWA is inherent to neural networks

We discovered that the diurnal cycle generates sleep need that elicits slow oscillatory activity within a previously described recurrent circuitry (Donlea et al., 2018). At night, the master sleep homeostat, the dFSB, increases excitability (Kempf et al., 2019) to generate compound oscillations (**Fig. 1**) which in turn promote partially coherent oscillatory activity in the sleep need mediating R5 network (**Fig. 1, 2**).

Interestingly, we found that dependent on the circadian clock the dFSB and the R5 network reciprocally facilitate presynaptic Ca^{2+} oscillations (**Fig. 2**) and propose the helicon cells (**Fig. 4**) as mediator between the networks. The diurnal variation in functional connectivity is most likely based on the R5 network's increase in presynaptic output weights when sleep need increases (Liu et al., 2016). The changes in synaptic weight might also promote the nighttime specific synchronization between helicon and R5 networks (**Fig. 4**), which we found to be an essential part of the filtering mechanism that promotes a quiescent egocentric mode (**Fig. 5**).

Similar to neural oscillations in mammalian circuits, we observed slight changes in the power spectrum of spontaneous SWA compared to the SWA induced by activating specific circuits. This is likely explained by the fact that the precise power and frequency of SWA depends on a complex interplay between different neural circuits (Neske, 2015). However, *ex vivo* recordings have shown that even relatively small isolated cortical and thalamic circuits have the ability to generate SWA (Neske, 2015), indicating that neural networks can oscillate autonomously. Moreover, the homeostatic regulation of SWA can occur locally in the brain, indicating that sleep need is experienced by specific networks (Huber et al., 2004). Our findings in *Drosophila* further substantiate the notion that SWA is inherent to neural circuits and that network coherence could represent an evolutionarily optimized strategy to create neural filter mechanisms (Raccuglia et al., 2019; Suárez-Grimalt and Raccuglia, 2021).

454 **Coherent network oscillations create a filter mechanism to promote quiescence**

455 Our data indicate that the dFSB acts as a switch that promotes oscillations in sleep need
456 mediating R5 (**Fig. 1, 2**) which in turn entrain oscillatory activity in arousal mediating helicon
457 (**Fig. 5**) thus promoting a quiescent state (**Fig. 3**) with reduced behavioral responsiveness (**Fig.**
458 **5**).

459 The observed network interactions have intriguing functional and physiological analogies to
460 thalamocortical interactions in mammalian brains. The thalamus orchestrates cortical
461 synchronization during sleep and functions as a relay station for sensory signals and motor
462 commands, essentially regulating behavioral responsiveness to external stimuli (Andrillon and
463 Kouider, 2020). However, how coherent oscillations can function as a gate remains unclear.

464 Here, our work provides mechanistic insight (**Fig. 7**): during the day, helicon and R5 act
465 independently of each other, allowing helicon to gate locomotion and update the heading
466 direction through excitation of EPG neurons (**Fig. 6**), which are part of a navigational system
467 that allows flies to orientate themselves in their surroundings (Kim et al., 2017; Seelig and
468 Jayaraman, 2013; Turner-Evans et al., 2017). At night, oscillating R5 neurons phase-lock
469 helicon activity in a slow rhythm (**Fig. 4, 5**). Here, our theoretical model recapitulates
470 synchronization of single R5 neurons (Raccuglia et al., 2019) and sets the R5 network as the
471 master oscillator to entrain helicon SWA (**Fig. 5**). The slow process of synchronization fits the
472 homeostatic build-up of sleep need over the time of day (Borbely, 1982) and potentially
473 increases the efficacy to filter out visual stimuli when synchronized by associating helicon. As
474 a consequence of coherent network activity, the functionally antagonistic inputs of helicon
475 and R5 to the head direction system cancel each other out (**Fig. 7**). Indeed, we show that
476 artificially imposing R5 activity at 1 Hz is sufficient to promote quiescence (**Fig. 3**) and impede
477 behavioral responsiveness (**Fig. 5**) to visual stimuli. Moreover, the inhibitory tone on EPG
478 neurons mediated by oscillating R5 neurons at night reduces the functional connectivity of
479 helicon to EPG, which might prevent updating of the heading direction and the initiation of
480 behavioral programs, effectively reducing behavioral responsiveness (**Fig. 7**). While similar
481 interactions have recently been proposed as part of a theoretical model (Flores-Valle et al.,
482 2021), we here provide experimental evidence for this, demonstrating that R5 and helicon
483 antagonistically regulate the head direction system (**Fig. 6**). Salient sensory stimuli might be
484 able to break up synchronized states by engaging additional neurons or specific engrams, thus
485 acutely increasing functional connectivity, which might lead to flies waking up and reacting to

external stimuli (French et al., 2021). We speculate that the neural interactions we discovered in this work are likely not restricted to flies, but could represent a neural filtering strategy (Tononi and Massimini, 2008) that correlates to a quiescent state less influenced by external cues, facilitating the shift from an allocentric-like to an egocentric-like worldview.

Neural networks integrating sleep need, navigation and postural control

One of the main functions of SWA during sleep has been shown to be the promotion of synaptic plasticity to consolidate experiences made during the day, providing the foundation for long-term memories (Klinzing et al., 2019). The circuitry we investigated in this work unifies visual processing, locomotion, navigation and sleep regulation. Ring neurons in general have been shown to play a role in visual place learning (Ofstad et al., 2011) and it is likely, that the oscillatory coherence reported here facilitates synaptic plasticity within the navigational system. Theoretical work has proposed that R5 could balance Hebbian plasticity in the navigational system by alternating between oscillatory and non-oscillatory states and by modulating the synaptic weights to head direction neurons (Fisher et al., 2019; Flores-Valle et al., 2021; Kim et al., 2019; Lu et al., 2022; Lyu et al., 2022; Vafidis et al., 2022).

Besides their role in navigation, we found that frequency-specific activation of R5 to mimic SWA induced a quiescent state accompanied by grooming (**Fig. 3**). Interestingly, we also observed frequent grooming during quiescence that occurred after a period of hyperactivity induced by artificial activation of the head direction system (**Fig. 6**), indicating that quiescence and grooming might be associated with each other. Indeed, grooming behavior in *Drosophila* is regulated by the circadian clock (Qiao et al., 2018) and occurs predominantly during short resting phases prior to night time sleep. Therefore, grooming could be considered as a transitioning stage for the egocentric mode (Qiao et al., 2018) and the activation of R5 might promote this preparatory stage eventually leading to sleep.

While optogenetic activation of R5 at 1 Hz induces quiescence, we found that activating R5 at 10 Hz can lead to a complete loss of postural control with flies falling over (**Fig. 3, 7**). Interestingly, flies also lost postural control when the head direction neurons were continuously hyperpolarized indicating that inhibitory control mediated by R5 SWA inhibits locomotion and provides the neurophysiological basis for maintaining postural control during

quiescence (**Fig. 7**). Moreover, SWA provides the temporal structure to create a 'breakable' filter, allowing strong or salient stimuli to 'break' the neural interaction and allow the animal to wake up. We propose that oscillatory patterns serve as incomplete 'road blocks' and allow for shutting off the route to the whole brain while not leading to unresponsiveness as observed in aberrant brain states such as coma. We therefore identified a network motif that not only mediates sleep regulation but also provides a system for the central regulation of postural control and locomotion-based behavioral programs.

525 **STAR METHODS**

526 **KEY RESOURCES TABLE**

REAGENT or RESOURCE	**SOURCE**	**IDENTIFIER**
Experimental models: Organisms/strains		
D. melanogaster:		
88F06-GAL4 (R5)	BDSC (Jenett et al., 2012)	BDSC: 40527
58H05-GAL4 (R5)	BDSC (Liu et al., 2016)	BDSC: 39198
58H05-LexA (R5)	BDSC (Liu et al., 2016)	BDSC: 61573
82F10-GAL4 (helicon)	BDSC (Jenett et al., 2012)	BDSC: 40336
24B11-GAL4 (helicon)	BDSC (Donlea et al., 2018)	BDSC: 49070
24B11-LexA (helicon)	BDSC (Donlea et al., 2018)	BDSC: 53547
23E10-GAL4 (dFSB)	BDSC (Donlea et al., 2014)	BDSC: 49032
23E10-LexA (dFSB)	BDSC (Donlea et al., 2014)	BDSC: 52693
60D05-GAL4 (EPG)	BDSC (Green et al., 2017)	BDSC: 39247
UAS-ArcLight	BDSC (Cao et al., 2013)	BDSC: 51056
LexAop-Varnam	BDSC (Kannan et al., 2018)	BDSC: 81937
LexAop-CsChrimson	BDSC(Sun et al., 2017)	BDSC: 55139
UAS-CsChrimson-tdTomato	BDSC (Klapoetke et al., 2014)	N/A
LexAop-P2X2R	BDSC (Claridge-Chang et al., 2009)	BDSC:
UAS-GCaMP6f	BDSC (Dana et al., 2019)	BDSC: 42747
UAS-GCaMP7b	BDSC (Dana et al., 2019)	BDSC: 80907
UAS-GtACR1 (imaging)	(Mohammad et al., 2017)	N/A
UAS-GtACR1-EYFP (behavior)	Gift from Alexander Borst (Mauss et al., 2017)	N/A
Chemicals		
All-*trans* retinal	Sigma-aldrich	R2500
Software and Algorithms		
Andor Solis	Andor	N/A
TriKinetics DAMSystem3	TriKinetics	RRID: SCR_021809

GraphPad Prism	GraphPad Software	RRID: SCR_002798
Python	Python	RRID: SCR_008394
Neuprint python	https://github.com/connectome-neuprint/neuprint-python	10.5281/zenodo.4968061
Navis	https://github.com/navis-org/navis	10.5281/zenodo.5710143
EzTrack	EzTrack (Pennington et al., 2019)	RRID: SCR_021496
BORIS	https://github.com/olivierfriard/BORIS (Friard and Gamba, 2016)	RRID: SCR_021434
Power Spectral Density	Matplotlib (matplotlib.pyplot.psd)	RRID:SCR_008624
Ramer-Douglas-Peucker	https://github.com/sebleier/RDP/	N/A

LEAD CONTACT AND MATERIALS AVAILABILITY

Requests for raw data, instrumentation and analysis code should be directed to the Lead Contact, David Owald (david.owald@charite.de). This study did not generate new unique reagents.

EXPERIMENTAL MODEL AND SUBJECT DETAILS

Flies (*Drosophila melanogaster*) were reared on standard cornmeal food at 25 °C and 60% humidity under a 12 h light/dark regime. Details of genotype and source of flies are given in **Key Resources Table**.

METHOD DETAILS

Imaging of neural activity

For voltage and Ca^{2+} imaging experiments we used 3-10 day old female flies and performed whole-brain explant dissections as previously described (Cao et al., 2013; Raccuglia et al., 2019). If not indicated otherwise, morning experiments were performed at ZT (Zeitgeber time) 2-4 (during a 12/12 h light/dark cycle the onset of light is at ZT 0 h and the offset of light is at ZT 12 h) and night experiments were performed at ZT 14-18.

To record spontaneous activity (**Fig. 1, 2G-I, 4, 6D**), we used a low Mg^{2+} external solution (5 mM) consisting of (in mM) 90 NaCl, 3 KCl, 1.5 $CaCl_2$, 5 $MgCl_2$, 1 NaH_2PO_4, 10 glucose, 10

549 sucrose, 8 trehalose, 5 TES and 26 $NaHCO_3$. To suppress spontaneous activity (**Fig 2A-F, 6G**)
550 we used a high Mg^{2+} external solution (20 mM) consisting of (in mM): 70 NaCl, 3 KCl, 1.5 $CaCl_2$,
551 20 $MgCl_2$, 1 NaH_2PO_4, 10 glucose, 10 sucrose, 8 trehalose, 5 TES and 26 $NaHCO_3$. To
552 compensate for Cl^- we adjusted NaCl concentration in the external solution, which did not
553 alter spontaneous activity (data not shown). External solution was adjusted to a pH of 7.4,
554 with an osmolarity of 280 mmol/kg.
555
556 Imaging was performed using an Olympus BX51WI microscope using a Plan Apochromat 40×,
557 numerical aperture 0.8, water-immersion objective (Olympus, Japan). The objective C-mount
558 image was projected onto an Andor iXon-888 camera controlled by Andor Solis software.
559 Voltage imaging was performed at ~80 frames/s while Ca^{2+} imaging was performed at ~20
560 frames/s. ArcLight and GCaMP were excited at 475/35 nm using a Lumencor Spectra X-Light
561 engine (Lumencor, USA) LED system. For Ca^{2+} imaging we used either GCaMP6f or GCaMP7b.
562 The increased brightness and sensitivity of GCaMP7b allows for an improved detection of
563 anatomical structures and neural activity in promotor lines with low baseline expression (Dana
564 et al., 2019). To avoid saturated fluorescent images, we adjusted the LED power for each
565 recording individually. To determine absolute fluorescence in single helicon cell bodies (**Fig.
566 S5-1D**) LED power was kept constant at 24% throughout all recordings. For dual color voltage
567 imaging, ArcLight and Varnam were simultaneously excited at 475/35 nm and 542/33 nm
568 using a Spectra X-Light engine LED (Lumencor, USA) system. For separating the emission
569 wavelengths, we used the W-View Gemini image splitter (Hamamatsu, Japan) with an
570 adequate dichroic mirror for ArcLight (520/35 nm) and Varnam (641/75 nm).
571 For dual-color voltage imaging and for optogenetic experiments, all-*trans* retinal (Sigma-
572 Aldrich) was added to the fly food as a 50 mM stock dissolved in 95 % ethanol. Female flies
573 were collected after eclosion and transferred to fly food containing 1.3 mM of all-trans retinal
574 for 2-4 days. CsChrimson was excited at 637/12 nm at a power density of 190-740 $\mu W/cm^2$.
575 For optogenetic hyperpolarization GtACR1 was excited at 542/33 nm at a similar power
576 density. Due to potential spectral overlap, excitation of ArcLight and GCaMP at 475/35 nm
577 was kept minimal (20-170 $\mu W/cm^2$). To reduce optical artefacts generated by red light
578 stimulation we used a custom-made dualband beamsplitter filter cube allowing red light to
579 pass the excitation filter but not the emission filter. To further reduce optical artifacts we

580 performed a background subtraction on imaging recordings (see quantification and statistical
581 analysis).
582
583 **Single-fly tracking experiments**
584 For measuring locomotor activity, we used female flies that were collected within 2-3 days
585 after eclosion. Experiments were performed in the dark in circular arenas (2.5 cm diameter)
586 illuminated from below using a low power infrared (850 nm) LED panel (2.7 mW/cm^2 at 520
587 nm). Flies were recorded from above at 15 frames/s using the high-resolution camera Flea3
588 USB3 (FL3-U3-13E4C-C, Teledyne FLIR) attached to a 25 mm focal length lens (#63-246,
589 Edmund Optics) and an infrared filter (10000314, Neewer) as done elsewhere (Aso and Rubin,
590 2016). For optogenetic experiments (**Fig. 3, 5** and **6**), flies were reared for 2-4 days after
591 collection in food supplemented with 1.3 mM all-*trans* retinal. To avoid optogenetic activation
592 during this time, vials containing flies were partially covered with a foil which still allowed
593 them to perceive background light. All experiments were carried out at room temperature
594 and during the subjective day of the fly (from ZT1-10).
595
596 At the start of each experiment, flies were allowed to acclimatize for 10 min. We then
597 measured the flies' initial baseline locomotor activity for 5 min (**Fig. 3B**). For optogenetic
598 activation experiments, flies were then exposed to 5 min of 5-ms pulses of red light (~20
599 mW/cm^2 at 632 nm) from below at a specific frequency indicated in the figure legends.
600 Subsequently locomotor activity was recorded for another 10 min. For optogenetic
601 hyperpolarization, flies were exposed to constant 1-min long green light from below (~9mW/
602 cm^2 at 520nm). For measuring absolute locomotor activity (distance travelled) and mean
603 velocities, we considered all movements. To determine whether flies were perturbed in their
604 ability to walk, we only considered velocities equal or higher than 0.25 cm/s (walking velocity
605 and % of time walking) (Donlea et al., 2018; Kottler et al., 2019). In order to normalize
606 locomotor variables to the baseline activity we computed the 'effect' of the optogenetic
607 protocol on baseline locomotion [ie. effect on total distance = (distance travelled during
608 stimulation – distance travelled during baseline) / (distance travelled during stimulation +
609 distance travelled during baseline)]. To evaluate turning behavior (**Fig. 6**), we simplified flies'
610 trajectories using an implementation of the Ramer-Douglas-Peucker algorithm
611 (https://github.com/sebleier/RDP/), computed the direction vectors of the simplified

612 trajectories and classified changes in direction equal or higher than 47º as turns. For high
613 resolution analysis of behavior during R5 activation and EPG inhibition experiments (**Fig. S3F,**
614 **G and S6D, E**), we manually annotated the occurrence of different behaviors: walking,
615 grooming, resting (flies are immobile with an upright body posture), loss of posture (flies are
616 immobile and upright body posture is lost) and recovering (flies are moving and trying to
617 recover upright body posture).
618

619 **Behavioral responsiveness**

620 To test visual responsiveness of sleep deprived flies (**Fig. 5F-H and S5I, J**), vials containing flies
621 reared in retinal food for 2-3 days were fixed to an analog Multi-Tube Vortexer (VX-2500,
622 VWR) controlled by TriKinetics acquisition software. For sleep deprivation a mechanical
623 stimulus lasting 2 s was provided randomly within a time window of 20 s from the beginning
624 of the subjective night (ZT 20) to the start of the experiment (ZT 1-7). Only sleep deprived flies
625 that did not move in the last 5 min of recording baseline activity (meeting the generally
626 accepted criteria for sleep) were included in the analysis. To assess visual responsiveness
627 during optogenetic activation flies were exposed to a 1-min green light stimulus from above
628 (0.37 mW/cm^2 measured at 520 nm). Responsiveness to light was evaluated by measuring
629 changes in a fly's velocity ('effect on mean velocity'). To determine whether flies were
630 awakened by light we only considered movements equal or higher than 0.25 cm/s.

631 To test responsiveness to an air puff during optogenetic activation (**Fig. S3D**), rested flies were
632 individually loaded in Trikinetics glass tubes (5x65 mm) connected to an air pump on one side
633 and sealed with perforated parafilm on the other end to allow air flow. Tubes were attached
634 to the LED panel for 1 Hz optogenetic activation and exposed to a constant 10 s air puff (~10
635 l/min) that was sufficiently strong to startle the flies. Responsiveness was measured by
636 comparing changes in mean velocity before and after the air puff (40 s each). To exclude
637 movements during the air puff, data 5 s before and after stimulus was not included in the
638 analysis.

639 **Network simulations**

640 To investigate the network configurations and mechanisms generating slow-wave oscillations
641 and networks coherence within and between R5 and helicon, we simulated network
642 interactions using a spiking neuron model introduced by Izhikevich (Izhikevich, 2003) (**Fig. 5**

643 and **Fig. S5-1**). For detailed description of the computational model, please see **Supplemental**
644 **Experimental Procedures**.
645

646 **Connectome analysis**

647 Neuronal types can be found in neuprint (neuprint.org) under the same name used in the
648 figures, with the exception of R neurons (ER5, ER4, etc. in the connectome) and helicon cells
649 (ExR1). The neuron type EPGt (Hulse et al., 2021) was not included in the EPG analysis. In the
650 connectivity plots, input weight contribution of a neuron (or set of neurons) *A* from a neuron
651 (or set of neurons) *B* refers to the number of synaptic connections that *A* receives from *B*,
652 normalized to the total number of input connections of *A*. Output weight contribution of *A* to
653 *B* refers to the number of output synaptic connections from *A* to *B*, normalized by the total
654 number of output connections of *A*. The 2D morphological renderings of neurons were
655 visualized using python. For the analysis of neighboring synapses in EPG neurons, we located
656 individual R5-to-EPG and helicon-to-EPG input connections in every EPG. Then, we identified
657 the closest input connection to each R5-to-EPG and helicon-to-EPG connection in the same
658 neuron (excluding other connections from R5 and helicon cells, respectively and connections
659 from cells not typed in the connectome). Distances between synaptic connections were
660 calculated using geodesic (along the arbor) distance.

661 **Visualization, software and statistics**

662 Activity recordings were analyzed using NOSA, a custom-made software specifically developed
663 to analyze voltage and Ca^{2+} imaging recordings (see https://github.com/DavideR2020/NOSA).
664 Relative fluorescence, background subtraction, power spectrum analysis and cross correlation
665 analysis were performed with algorithms described in detail previously (Oltmanns et al., 2020;
666 Raccuglia et al., 2019). From NOSA, data sets were exported to Microsoft Excel for further
667 analysis. For visualization of experimental data, we used CorelDRAW2020. For a more intuitive
668 display, all ArcLight and Varnam recordings are inverted, as depolarization leads to a decrease
669 in fluorescence intensity while hyperpolarization leads to an increase. For power spectrum
670 analysis, the unit of the power spectral density (PSD) is indicated as PSD = $[(\Delta F/F)^2 /Hz] *100$.
671 To quantify response amplitudes during optogenetic activation (**Fig. 6H**) we computed the
672 difference of the average relative change in fluorescence intensity during and before

673 optogenetic stimulation. All imaging data are presented as means with standard error of the
674 mean (SEM).
675
676 For tracking recordings, single fly position data was extracted from videos using EzTrack
677 (Pennington et al., 2019) (https://github.com/denisecailab/ezTrack). Hemibrain connectome
678 data (version 2.1) (Scheffer et al., 2020) was accessed using neuprint-python
679 (https://github.com/connectome-neuprint/neuprint-python) and geodesic (along the arbor)
680 distances between synaptic connections were calculated using navis
681 (https://github.com/navis-org/navis). Manual annotation of behaviors was performed using
682 BORIS (https://github.com/olivierfriard/BORIS) (Friard and Gamba, 2016). Behavioral and
683 connectome data were analyzed using custom-made python scripts. In behavioral panels,
684 box-plots show median (line), quartiles (boxes) and range (whiskers) and locomotor activity
685 curves indicate mean ± SEM. Behavioral and connectome data were visualized using python.
686
687 R5 and helicon network simulations were performed, analysed and visualized using python.

688 Statistical analysis was carried out in GraphPad Prism. In all panels, significance is represented
689 as follows: *$p \leq 0.05$, **$p \leq 0.01$, ***$p \leq 0.001$ and ns (not significant). The statistical tests
690 performed in each panel are indicated in the figure legends. For unpaired comparisons, we
691 used Mann-Whitney test when comparing 2 groups and Kruskal-Wallis test with Dunn's post
692 hoc analysis for multiple comparisons. For paired comparisons, we used Wilxocon matched
693 pairs signed rank test when comparing 2 groups and Friedman test with Dunn's post hoc
694 analysis for multiple comparisons. Comparisons to 0 were performed using Wilcoxon signed-
695 ranked tests and percentages were compared using Binomial test.

696 **DATA AND CODE AVAILABILITY**

697 Raw data are available from the corresponding author upon reasonable request.

698
699
700

Acknowledgements

We thank Peter Spende, Alexej Schatz, Waldemar Krzok, Raz Flieshman, Karim Izzuldin and Katharina Stumpenhorst for help with the behavioral arena; Johannes Felsenberg and members of the Owald lab for comments on the manuscript, Scidraw for allowing us to modify and use their schematics (fly drawing: doi.org/10.5281/zenodo.3926137) and Alexander Borst, the Janelia fly line project and Bloomington Stock Center for flies.

Funding

This project was funded by the Deutsche Forschungsgemeinschaft (DFG, German Research Foundation) under Germany´s Excellence Strategy – EXC-2049 – 390688087, the Emmy Noether Programme and TP A27 of SFB958 (184695641) to DO and TP A07, B01 and C02 of SFB1315 (327654276) to D.O, R.K. and Y.W. D.O. was further supported by FOR 2705 (365082554). D.R. was supported by the DFG grant 462539941. R.S-G. and L.K. were supported by an Einstein Center for Neurosciences Berlin PhD fellowship. S.R.J. was supported by the DFG grant 467545627.

Author contribution:

Conceptualization: D.R., R.S-G., L.K., R.K. and D.O.

Investigation: D.R., R.S-G., L.K, A.E., C.B., S.R.J, and G. Y-D.

Resources: D.R., Y.W, R.K., J.R.G. and D.O.

Writing – Original Draft: D.R., R.S-G., L.K., R.K. and D.O.

Writing – Review & Editing: A.E, C.B. and J.R.G.

Authors declare no competing interests.

References

Adamantidis, A.R., Gutierrez Herrera, C., and Gent, T.C. (2019). Oscillating circuitries in the sleeping brain. Nat Rev Neurosci *20*, 746-762.

Aleman, A., Omoto, J.J., Singh, P., Nguyen, B.-C., Kandimalla, P., Hartenstein, V., and Donlea, J.M. (2021). Opposing subclasses of Drosophila ellipsoid body neurons promote and suppress sleep. bioRxiv, 2021.2010.2019.464469.

Andrillon, T., and Kouider, S. (2020). The vigilant sleeper: neural mechanisms of sensory (de)coupling during sleep. Current Opinion in Physiology *15*, 47-59.

Aso, Y., and Rubin, G.M. (2016). Dopaminergic neurons write and update memories with cell-type-specific rules. Elife *5*.

Barker, J.L., and Harrison, N.L. (1988). Outward rectification of inhibitory postsynaptic currents in cultured rat hippocampal neurones. J Physiol *403*, 41-55.

Blum, I.D., Keles, M.F., Baz, E.S., Han, E., Park, K., Luu, S., Issa, H., Brown, M., Ho, M.C.W., Tabuchi, M.*, et al.* (2021). Astroglial Calcium Signaling Encodes Sleep Need in Drosophila. Curr Biol *31*, 150-162 e157.

Borbely, A.A. (1982). A two process model of sleep regulation. Hum Neurobiol *1*, 195-204.

Buzsaki, G., and Draguhn, A. (2004). Neuronal oscillations in cortical networks. Science *304*, 1926-1929.

Cao, G., Platisa, J., Pieribone, V.A., Raccuglia, D., Kunst, M., and Nitabach, M.N. (2013). Genetically targeted optical electrophysiology in intact neural circuits. Cell *154*, 904-913.

Claridge-Chang, A., Roorda, R.D., Vrontou, E., Sjulson, L., Li, H., Hirsh, J., and Miesenbock, G. (2009). Writing memories with light-addressable reinforcement circuitry. Cell *139*, 405-415.

Crunelli, V., and Hughes, S.W. (2010). The slow (<1 Hz) rhythm of non-REM sleep: a dialogue between three cardinal oscillators. Nat Neurosci *13*, 9-17.

Dana, H., Sun, Y., Mohar, B., Hulse, B.K., Kerlin, A.M., Hasseman, J.P., Tsegaye, G., Tsang, A., Wong, A., Patel, R.*, et al.* (2019). High-performance calcium sensors for imaging activity in neuronal populations and microcompartments. Nat Methods *16*, 649-657.

Donlea, J.M. (2019). Roles for sleep in memory: insights from the fly. Curr Opin Neurobiol *54*, 120-126.

Donlea, J.M., Pimentel, D., and Miesenbock, G. (2014). Neuronal machinery of sleep homeostasis in Drosophila. Neuron *81*, 860-872.

Donlea, J.M., Pimentel, D., Talbot, C.B., Kempf, A., Omoto, J.J., Hartenstein, V., and Miesenbock, G. (2018). Recurrent Circuitry for Balancing Sleep Need and Sleep. Neuron *97*, 378-389 e374.

Donlea, J.M., Ramanan, N., and Shaw, P.J. (2009). Use-dependent plasticity in clock neurons regulates sleep need in Drosophila. Science *324*, 105-108.

Fayyazuddin, A., Zaheer, M.A., Hiesinger, P.R., and Bellen, H.J. (2006). The nicotinic acetylcholine receptor Dalpha7 is required for an escape behavior in Drosophila. PLoS Biol *4*, e63.

Fisher, Y.E., Lu, J., D'Alessandro, I., and Wilson, R.I. (2019). Sensorimotor experience remaps visual input to a heading-direction network. Nature *576*, 121-125.

Flores-Valle, A., Goncalves, P.J., and Seelig, J.D. (2021). Integration of sleep homeostasis and navigation in Drosophila. PLoS Comput Biol *17*, e1009088.

French, A.S., Geissmann, Q., Beckwith, E.J., and Gilestro, G.F. (2021). Sensory processing during sleep in Drosophila melanogaster. Nature *598*, 479-482.

Friard, O., and Gamba, M. (2016). BORIS: a free, versatile open-source event-logging software for video/audio coding and live observations. Methods in Ecology and Evolution *7*, 1325-1330.

Gent, T.C., Bandarabadi, M., Herrera, C.G., and Adamantidis, A.R. (2018). Thalamic dual control of sleep and wakefulness. Nat Neurosci *21*, 974-984.

Green, J., Adachi, A., Shah, K.K., Hirokawa, J.D., Magani, P.S., and Maimon, G. (2017). A neural circuit architecture for angular integration in Drosophila. Nature *546*, 101-106.

Hanesch, U., Fischbach, K.F., and Heisenberg, M. (1989). Neuronal architecture of the central complex in Drosophila melanogaster. Cell and Tissue Research *257*, 343-366.

Huang, S., Piao, C., Beuschel, C.B., Gotz, T., and Sigrist, S.J. (2020). Presynaptic Active Zone Plasticity Encodes Sleep Need in Drosophila. Curr Biol *30*, 1077-1091 e1075.

Huber, R., Ghilardi, M.F., Massimini, M., and Tononi, G. (2004). Local sleep and learning. Nature *430*, 78-81.

Hulse, B.K., Haberkern, H., Franconville, R., Turner-Evans, D.B., Takemura, S.Y., Wolff, T., Noorman, M., Dreher, M., Dan, C., Parekh, R.*, et al.* (2021). A connectome of the Drosophila central complex reveals network motifs suitable for flexible navigation and context-dependent action selection. Elife *10*.

Hung, C.S., Sarasso, S., Ferrarelli, F., Riedner, B., Ghilardi, M.F., Cirelli, C., and Tononi, G. (2013). Local experience-dependent changes in the wake EEG after prolonged wakefulness. Sleep *36*, 59-72.

Izhikevich, E.M. (2003). Simple model of spiking neurons. IEEE Trans Neural Netw *14*, 1569-1572.

Jenett, A., Rubin, G.M., Ngo, T.T., Shepherd, D., Murphy, C., Dionne, H., Pfeiffer, B.D., Cavallaro, A., Hall, D., Jeter, J.*, et al.* (2012). A GAL4-driver line resource for Drosophila neurobiology. Cell Rep *2*, 991-1001.

Kannan, M., Vasan, G., Huang, C., Haziza, S., Li, J.Z., Inan, H., Schnitzer, M.J., and Pieribone, V.A. (2018). Fast, in vivo voltage imaging using a red fluorescent indicator. Nat Methods *15*, 1108-1116.

Kempf, A., Song, S.M., Talbot, C.B., and Miesenbock, G. (2019). A potassium channel beta-subunit couples mitochondrial electron transport to sleep. Nature *568*, 230-234.

Kim, S.S., Hermundstad, A.M., Romani, S., Abbott, L.F., and Jayaraman, V. (2019). Generation of stable heading representations in diverse visual scenes. Nature *576*, 126-131.

Kim, S.S., Rouault, H., Druckmann, S., and Jayaraman, V. (2017). Ring attractor dynamics in the Drosophila central brain. Science *356*, 849-853.

Klapoetke, N.C., Murata, Y., Kim, S.S., Pulver, S.R., Birdsey-Benson, A., Cho, Y.K., Morimoto, T.K., Chuong, A.S., Carpenter, E.J., Tian, Z.*, et al.* (2014). Independent optical excitation of distinct neural populations. Nat Methods *11*, 338-346.

Klinzing, J.G., Niethard, N., and Born, J. (2019). Mechanisms of systems memory consolidation during sleep. Nat Neurosci *22*, 1598-1610.

Kottler, B., Faville, R., Bridi, J.C., and Hirth, F. (2019). Inverse Control of Turning Behavior by Dopamine D1 Receptor Signaling in Columnar and Ring Neurons of the Central Complex in Drosophila. Curr Biol *29*, 567-577 e566.

Krueger, J.M., Nguyen, J.T., Dykstra-Aiello, C.J., and Taishi, P. (2019). Local sleep. Sleep Med Rev *43*, 14-21.

Lamaze, A., Kratschmer, P., Chen, K.F., Lowe, S., and Jepson, J.E.C. (2018). A Wake-Promoting Circadian Output Circuit in Drosophila. Curr Biol *28*, 3098-3105 e3093.

Leung, L.C., Wang, G.X., Madelaine, R., Skariah, G., Kawakami, K., Deisseroth, K., Urban, A.E., and Mourrain, P. (2019). Neural signatures of sleep in zebrafish. Nature *571*, 198-204.

Liu, S., Liu, Q., Tabuchi, M., and Wu, M.N. (2016). Sleep Drive Is Encoded by Neural Plastic Changes in a Dedicated Circuit. Cell *165*, 1347-1360.

Low, P.S., Shank, S.S., Sejnowski, T.J., and Margoliash, D. (2008). Mammalian-like features of sleep structure in zebra finches. Proc Natl Acad Sci U S A *105*, 9081-9086.

Lu, J., Behbahani, A.H., Hamburg, L., Westeinde, E.A., Dawson, P.M., Lyu, C., Maimon, G., Dickinson, M.H., Druckmann, S., and Wilson, R.I. (2022). Transforming representations of movement from body- to world-centric space. Nature *601*, 98-104.

Lyu, C., Abbott, L.F., and Maimon, G. (2022). Building an allocentric travelling direction signal via vector computation. Nature *601*, 92-97.

Mauss, A.S., Busch, C., and Borst, A. (2017). Optogenetic Neuronal Silencing in Drosophila during Visual Processing. Sci Rep *7*, 13823.

Mohammad, F., Stewart, J.C., Ott, S., Chlebikova, K., Chua, J.Y., Koh, T.W., Ho, J., and Claridge-Chang, A. (2017). Optogenetic inhibition of behavior with anion channelrhodopsins. Nat Methods *14*, 271-274.

Neske, G.T. (2015). The Slow Oscillation in Cortical and Thalamic Networks: Mechanisms and Functions. Front Neural Circuits *9*, 88.

Ofstad, T.A., Zuker, C.S., and Reiser, M.B. (2011). Visual place learning in Drosophila melanogaster. Nature *474*, 204-207.

Oltmanns, S., Abben, F.S., Ender, A., Aimon, S., Kovacs, R., Sigrist, S.J., Storace, D.A., Geiger, J.R.P., and Raccuglia, D. (2020). NOSA, an Analytical Toolbox for Multicellular Optical Electrophysiology. Front Neurosci *14*, 712.

Pankova, K., and Borst, A. (2017). Transgenic line for the identification of cholinergic release sites in Drosophila melanogaster. J Exp Biol *220*, 1405-1410.
Pennington, Z.T., Dong, Z., Feng, Y., Vetere, L.M., Page-Harley, L., Shuman, T., and Cai, D.J. (2019). ezTrack: An open-source video analysis pipeline for the investigation of animal behavior. Sci Rep *9*, 19979.
Pimentel, D., Donlea, J.M., Talbot, C.B., Song, S.M., Thurston, A.J.F., and Miesenbock, G. (2016). Operation of a homeostatic sleep switch. Nature *536*, 333-337.
Qiao, B., Li, C., Allen, V.W., Shirasu-Hiza, M., and Syed, S. (2018). Automated analysis of long-term grooming behavior in Drosophila using a k-nearest neighbors classifier. Elife *7*.
Quercia, A., Zappasodi, F., Committeri, G., and Ferrara, M. (2018). Local Use-Dependent Sleep in Wakefulness Links Performance Errors to Learning. Front Hum Neurosci *12*, 122.
Raccuglia, D., Huang, S., Ender, A., Heim, M.M., Laber, D., Suarez-Grimalt, R., Liotta, A., Sigrist, S.J., Geiger, J.R.P., and Owald, D. (2019). Network-Specific Synchronization of Electrical Slow-Wave Oscillations Regulates Sleep Drive in Drosophila. Curr Biol *29*, 3611-3621 e3613.
Raccuglia, D., McCurdy, L.Y., Demir, M., Gorur-Shandilya, S., Kunst, M., Emonet, T., and Nitabach, M.N. (2016). Presynaptic GABA Receptors Mediate Temporal Contrast Enhancement in Drosophila Olfactory Sensory Neurons and Modulate Odor-Driven Behavioral Kinetics. eNeuro *3*.
Ramon, F., Hernandez-Falcon, J., Nguyen, B., and Bullock, T.H. (2004). Slow wave sleep in crayfish. Proc Natl Acad Sci U S A *101*, 11857-11861.
Sanchez-Vives, M.V., and McCormick, D.A. (2000). Cellular and network mechanisms of rhythmic recurrent activity in neocortex. Nat Neurosci *3*, 1027-1034.
Scheffer, L.K., Xu, C.S., Januszewski, M., Lu, Z., Takemura, S.Y., Hayworth, K.J., Huang, G.B., Shinomiya, K., Maitlin-Shepard, J., Berg, S.*, et al.* (2020). A connectome and analysis of the adult Drosophila central brain. Elife *9*.
Seelig, J.D., and Jayaraman, V. (2013). Feature detection and orientation tuning in the Drosophila central complex. Nature *503*, 262-266.
Shaw, P.J., Cirelli, C., Greenspan, R.J., and Tononi, G. (2000). Correlates of sleep and waking in Drosophila melanogaster. Science *287*, 1834-1837.
Shein-Idelson, M., Ondracek, J.M., Liaw, H.P., Reiter, S., and Laurent, G. (2016). Slow waves, sharp waves, ripples, and REM in sleeping dragons. Science *352*, 590-595.
Siclari, F., and Tononi, G. (2017). Local aspects of sleep and wakefulness. Curr Opin Neurobiol *44*, 222-227.
Suárez-Grimalt, R., and Raccuglia, D. (2021). The neural architecture of sleep regulation – insights from Drosophila. Neuroforum *27*, 189-199.
Sun, Y., Nern, A., Franconville, R., Dana, H., Schreiter, E.R., Looger, L.L., Svoboda, K., Kim, D.S., Hermundstad, A.M., and Jayaraman, V. (2017). Neural signatures of dynamic stimulus selection in Drosophila. Nat Neurosci *20*, 1104-1113.
Terman, D., Kopell, N., and Bose, A. (1998). Dynamics of two mutually coupled slow inhibitory neurons. Physica D: Nonlinear Phenomena *117*, 241-275.
Tononi, G., and Massimini, M. (2008). Why does consciousness fade in early sleep? Ann N Y Acad Sci *1129*, 330-334.
Troup, M., Yap, M.H., Rohrscheib, C., Grabowska, M.J., Ertekin, D., Randeniya, R., Kottler, B., Larkin, A., Munro, K., Shaw, P.J.*, et al.* (2018). Acute control of the sleep switch in Drosophila reveals a role for gap junctions in regulating behavioral responsiveness. Elife *7*.
Turner-Evans, D., Wegener, S., Rouault, H., Franconville, R., Wolff, T., Seelig, J.D., Druckmann, S., and Jayaraman, V. (2017). Angular velocity integration in a fly heading circuit. Elife *6*.
Vafidis, P., Owald, D., D'Albis, T., and Kempter, R. (2022). Learning accurate path integration in ring attractor models of the head direction system. Elife *11*.
Vyazovskiy, V.V., Olcese, U., Hanlon, E.C., Nir, Y., Cirelli, C., and Tononi, G. (2011). Local sleep in awake rats. Nature *472*, 443-447.

Yap, M.H.W., Grabowska, M.J., Rohrscheib, C., Jeans, R., Troup, M., Paulk, A.C., van Alphen, B., Shaw, P.J., and van Swinderen, B. (2017). Oscillatory brain activity in spontaneous and induced sleep stages in flies. Nat Commun *8*, 1815.

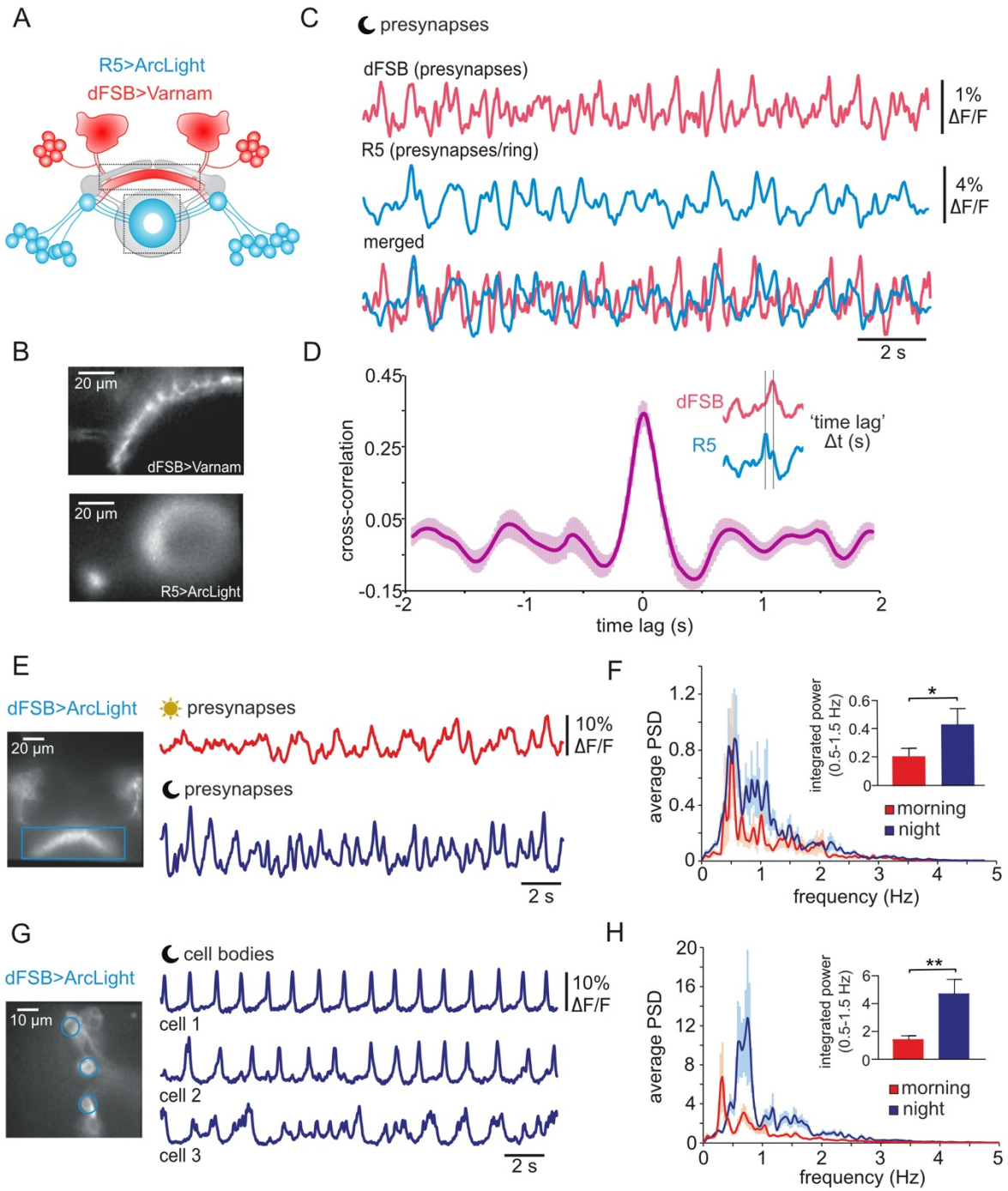

Figure 1. Neural circuits mediating sleep drive display slow-wave coherence.
(A) Schematic of a sleep regulating circuitry composed of dorsal fan-shaped body (dFSB, red), helicon cells (grey) and R5 neurons (blue). dFSB and R5 neurons are highlighted to indicate expression of genetically encoded voltage indicators (GEVIs). Rectangles indicate recording sites. **(B)** Wide-field image of dFSB neurons expressing Varnam (23E10-LexA) and R5 neurons simultaneously expressing ArcLight (88F06-GAL4). **(C)** Example recording of R5 and dFSB electrical patterns recorded at night (ZT 14-15). **(D)** Cross correlogram of electrical patterns of R5 and dFSB (*n*=10) indicates an overlap of electrical patterns. **(E)** Wide-field image of dFSB neurites and compound recordings of presynaptic electrical activity recorded in the morning (ZT 2-4) and at night (ZT 14-15). **(F)** Average power spectra of compound oscillations in dFSB presynapses. Compound integrated slow-wave power (0.5-1.5 Hz) is increased at night (*n*=9-

10, Mann-Whitney test). **(G)** Multi-cellular voltage imaging of individual dFSB neurons recorded in the morning (ZT 2-4) and at night (ZT 14-15). **(H)** Average power spectrum of single-cell voltage recordings showing increased slow-wave power (0.5-1.5 Hz) at night (*n*=23 for ZT 2-4 and *n*=34 for ZT 14-15, Mann-Whitney test).

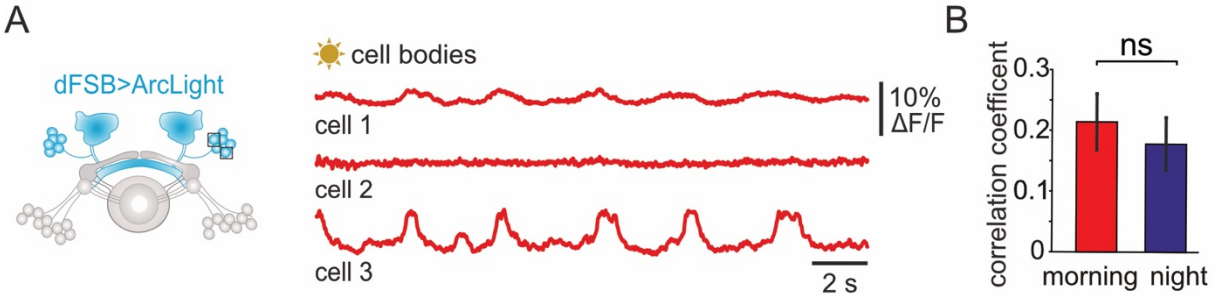

Figure S1 (A) *Ex vivo* multi-cellular voltage imaging of individual dFSB neurons recorded in the morning (ZT 2-4). Squares schematically indicate recording sites. **(B)** Correlation between electrical patterns of individual cell bodies is similar in the morning and at night (*n*=30-39, Mann-Whitney test).

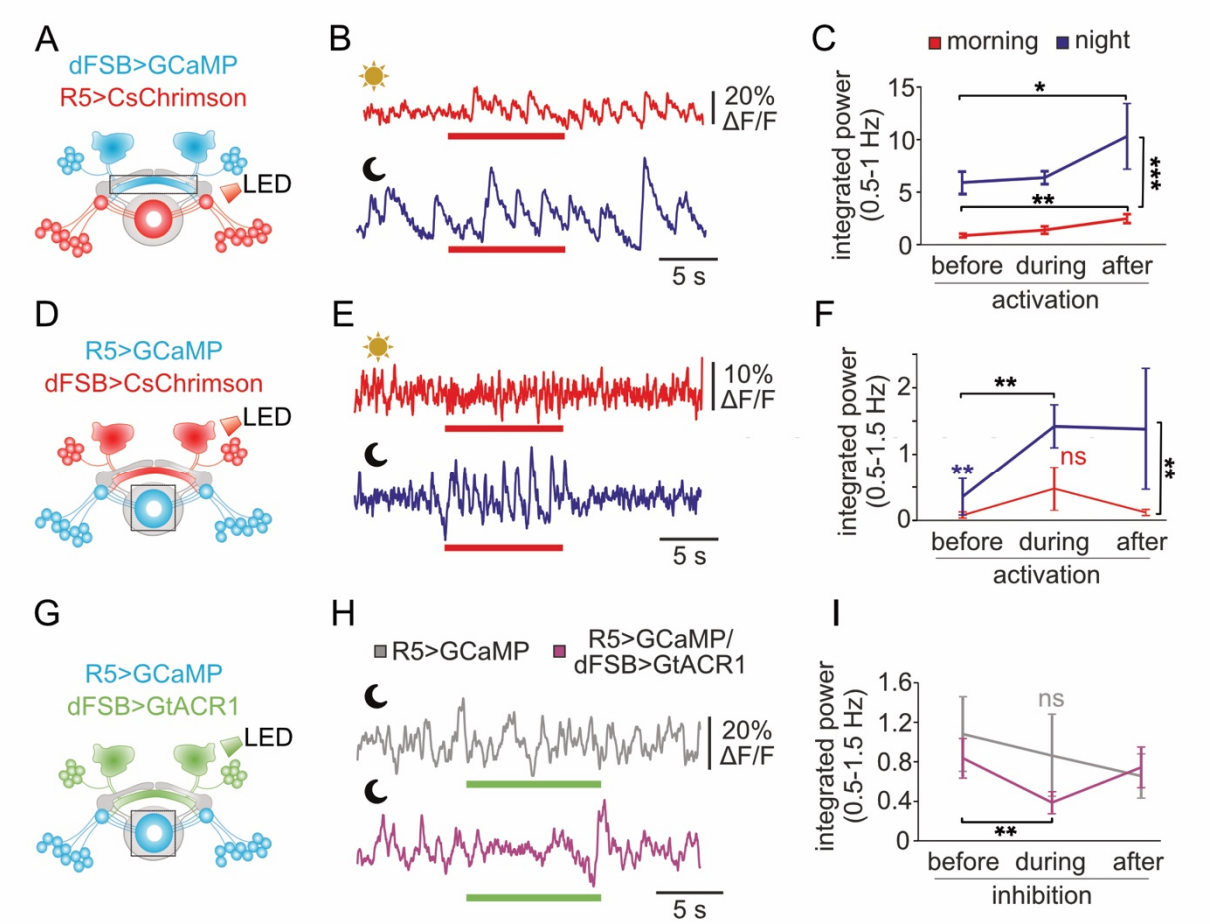

Figure 2: Reciprocal facilitation of SWA between sleep drive mediating circuits is modulated by the circadian clock.

(A, D, G) Schematic overview of presynaptic recording sites and sites of optogenetic activation and inhibition. **(B)** Example traces of dFSB presynaptic Ca^{2+} activity (23E10-GAL4) during optogenetic activation (red bars) of R5 neurons (58H05-LexA) in the morning (ZT 2-6) and at night (ZT 14-18). **(C)** Slow-wave power (0.5-1 Hz) in the dFSB increases after optogenetic stimulation of R5 neurons (*n*=10, Friedman test with post hoc Dunn's multiple comparisons test). Pooling the data for during and after stimulation indicates that inducing oscillations is facilitated at night (*n*=20, Mann-Whitney test). **(E)** Example traces of R5 presynaptic Ca^{2+} activity (58H05-GAL4) during optogenetic activation of dFSB neurons (23E10-LexA) in the morning (ZT 2-6) and at night (ZT 14-18). **(F)** At night but not in the morning R5 slow-wave power (0.5-1.5 Hz) increases during optogenetic stimulation of R5 neurons (*n*=10-11, Friedman test with post hoc Dunn's multiple comparisons test). Pooling the data for during and after stimulation indicates that the induction of oscillations is facilitated at night (*n*=20-22, Mann-Whitney test). **(H)** Example traces of R5 presynaptic Ca^{2+} activity (58H05-LexA) during optogenetic inhibition of dFSB neurons (23E10-GAL4) at nighttime. **(I)** Slow-wave power (0.5-1.5 Hz) is reduced when hyperpolarizing dFSB neurons (*n*=6-7, Friedman test with post hoc Dunn's multiple comparisons test).

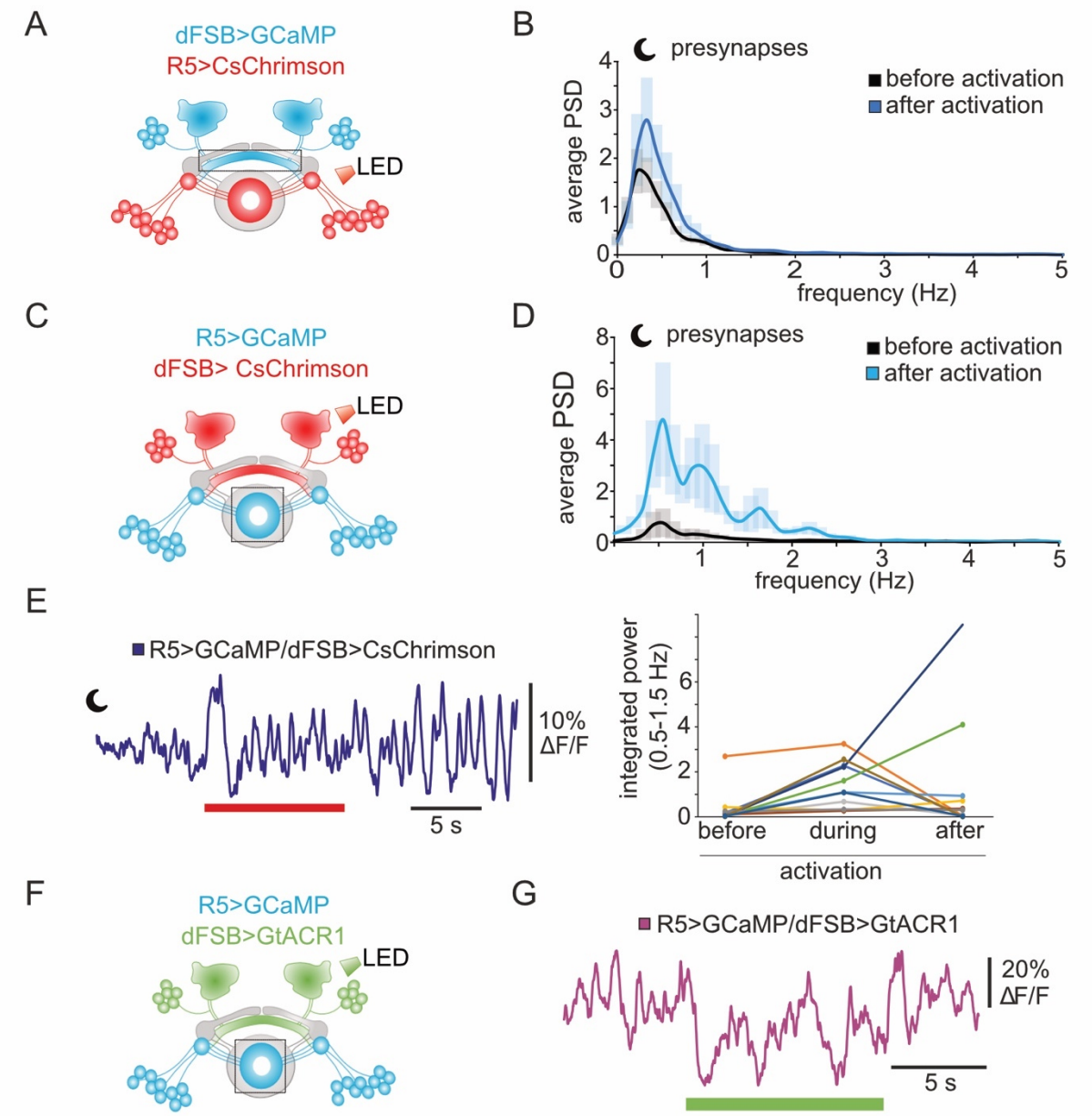

Figure S2. (A, C) Schematic overview of presynaptic recording sites and sites of optogenetic activation. **(B)** Average power spectra of dFSB compound oscillations before and after optogenetic stimulation of R5 (*n*=10). **(D)** Average power spectra of R5 compound oscillations before and during optogenetic stimulation of dFSB neurons (*n*=11). **(E)** Left: example recording of ongoing R5 presynaptic Ca^{2+} oscillations after cessation of dFSB stimulation. Right: individual data points of R5 slow-wave power (0.5-1.5 Hz) show that in some cases R5 oscillations persist after cessation of dFSB stimulation. **(F)** Schematic overview indicating expression of GtACR1 in dFSB and Ca^{2+} recording sites at the R5 ring. **(G)** Example recording of R5 presynaptic Ca^{2+} activity showing partially recovering oscillatory activity during optogenetic inhibition of dFSB neurons.

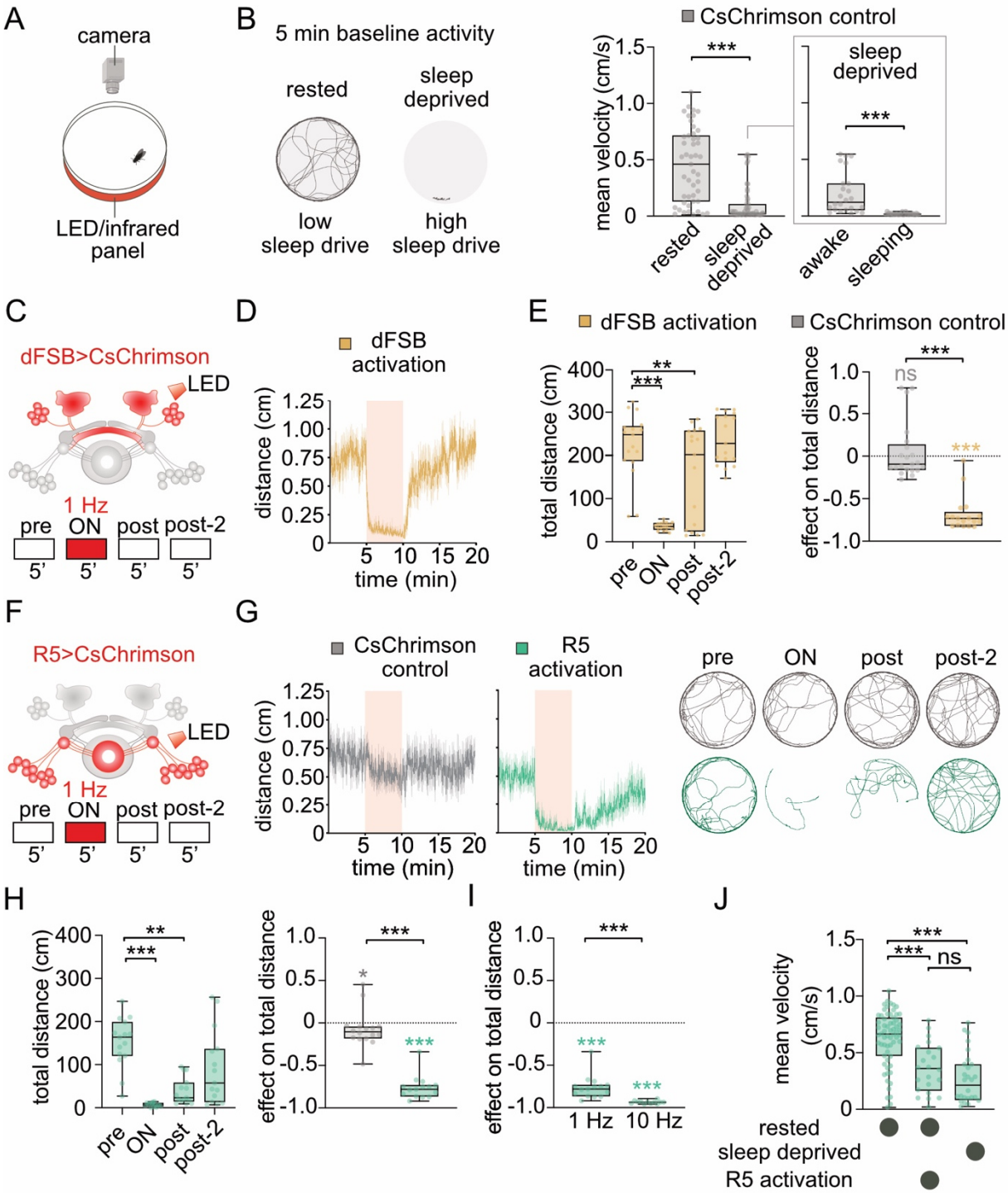

Figure 3. Neural circuits mediating sleep drive acutely control locomotor behavior.
(A) Locomotor activity is assessed by continuously tracking the position of a single fly in a circular arena. **(B)** Locomotor activity of individual flies correlates to the internal sleep drive. Left: example trajectories (5 min) of a rested and a sleep deprived fly (+>LexAop-CsChrimson). Right: baseline velocity of sleep-deprived flies is reduced compared to that of rested flies (*n*=43 for rested and *n*=55 for sleep deprived, Mann-Whitney test). Sleep deprived flies either meet the sleep criteria (5 min of inactivity, 'sleeping', *n*=31) or are active ('awake', *n*=24). **(C)** Schematic overview of the optogenetic protocol used to activate dFSB under 23E10-GAL4 control. After 5 min of baseline activity ('pre'), rested flies were exposed to 5 min red light at 1 Hz ('ON') and allowed to recover for 10 min ('post' and 'post-2'). **(D)** Average locomotion trace of 23E10-GAL4>UAS-CsChrimson flies (+ retinal, *n*=17). Curves: mean ± SEM. **(E)** Left: 1

992 Hz dFSB activation decreases locomotion of rested flies during and after activation (*n*=17,
993 Friedman test with Dunn's multiple comparisons). Right: optogenetic stimulation of the dFSB
994 (+ retinal) reduced total distance travelled compared to control flies (+ retinal), *n*=17-19,
995 Mann-Whitney test (comparisons between genotypes depicted in black) and Wilcoxon signed-
996 rank test (comparisons to baseline locomotion depicted in color). **(F)** The same optogenetic
997 protocol described in **C** is used to activate R5 neurons under 58H05-GAL4 control. **(G)** Left:
998 average locomotion traces of CsChrimson control (+ retinal, *n*=16) and 58H05-GAL4>UAS-
999 CsChrimson flies (+ retinal, *n*=15). Curves: mean ± SEM. Right: example trajectories. **(H)** Left:
1000 1 Hz stimulation reduced distance travelled during and after activation of R5 (*n*=15, Friedman
1001 test with Dunn's multiple comparisons). Right: optogenetic activation of R5 decreased
1002 distance travelled compared to control flies, *n*=15-16 each group, Mann-Whitney test
1003 (comparisons between genotypes depicted in black) and Wilcoxon signed-rank test
1004 (comparisons to baseline locomotion depicted in color). **(I)** The effect of R5 stimulation on
1005 distance travelled differed between different activation frequencies (*n*=15 for 1 Hz and *n*=12
1006 for 10 Hz, Mann-Whitney test). **(J)** Mean walking velocity was reduced when R5 was activated
1007 at 1 Hz, resembling the locomotion levels of awake but sleep-deprived flies (+ retinal) (*n*=63
1008 for rested, *n*=22 for rested+R5 activation, *n*=28 for sleep deprived, Kruskal-Wallis test with
1009 Dunn's multiple comparisons). Experiments shown in this figure were performed during the
1010 subjective day of the flies (ZT 1-10).
1011

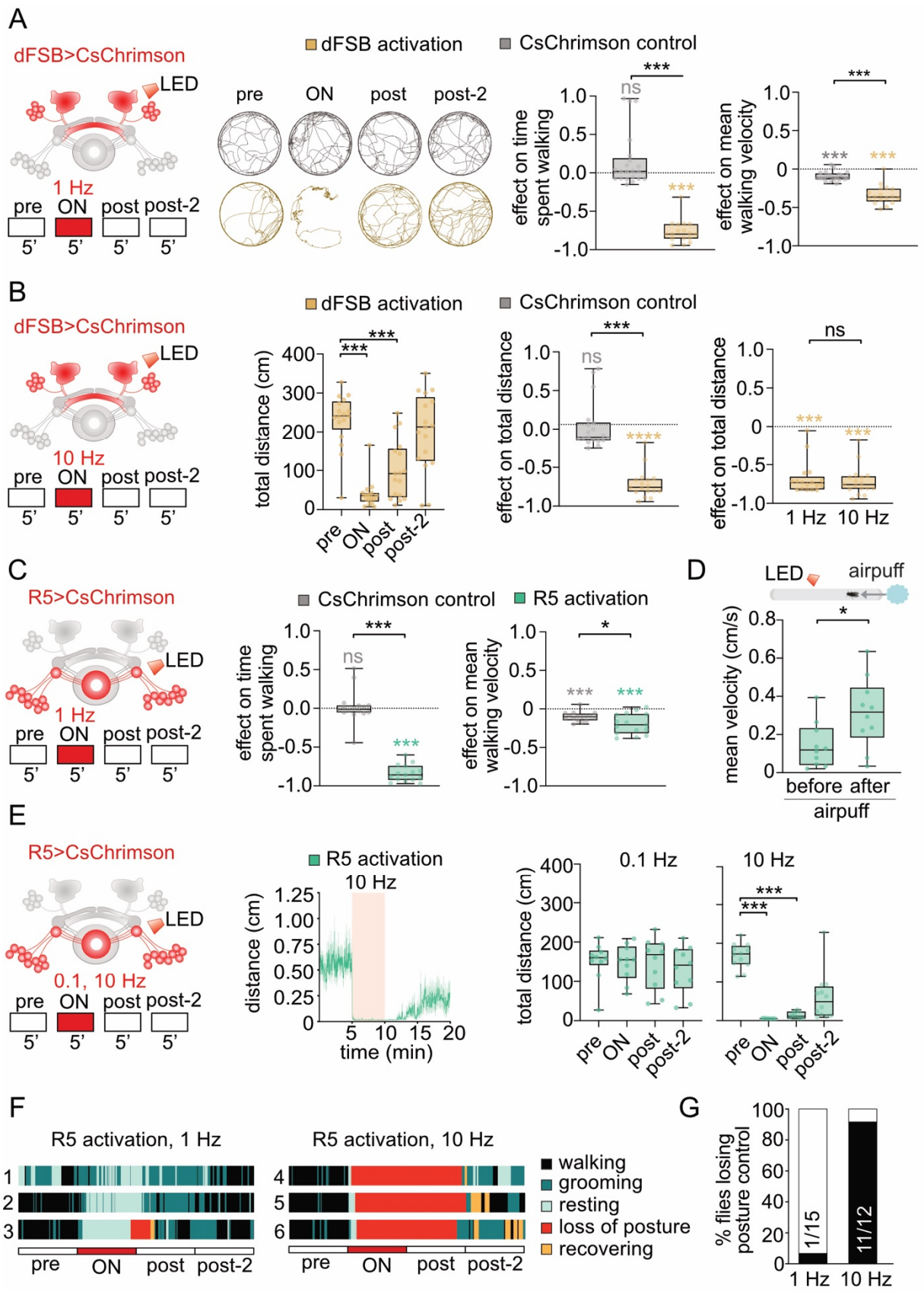

Figure S3.

(A) Optogenetic stimulation of dFSB neurons at 1 Hz using the protocol described in Fig. 3C. Example trajectories of CsChrimson control (+ retinal) and 23E10-GAL4>UAS-CsChrimson (+ retinal) flies. Optogenetic stimulation of dFSB neurons at 1 Hz in rested flies decreased

1017 percentage of time walking and mean walking velocity compared to control flies, *n*=17-19 each
1018 group, Mann-Whitney test (comparisons between genotypes depicted in black) and Wilcoxon
1019 signed-rank test (comparisons to baseline locomotion depicted in color). **(B)** Activation of dFSB
1020 at 10 Hz decreased total distance travelled during and after activation (*n*=17, Friedman test
1021 with Dunn's multiple comparisons). The effect of dFSB stimulation at 10 Hz on distance
1022 travelled differed to that of control flies, *n*=17-19 each group, Mann-Whitney test
1023 (comparisons between genotypes depicted in black) and Wilcoxon signed-rank test
1024 (comparisons to baseline locomotion depicted in color). The effect of dFSB stimulation on
1025 distance travelled did not differ between different frequencies of activation (*n*= 17 each,
1026 Mann-Whitney test). **(C)** Activation of R5 neurons at 1 Hz in rested flies expressing CsChrimson
1027 under 58H05-GAL4 control (+ retinal) decreased percentage of time walking and mean walking
1028 velocity compared to control flies, *n*=15-16 each group, Mann-Whitney test (comparisons
1029 between genotypes depicted in black) and Wilcoxon signed-rank test (comparisons to baseline
1030 locomotion depicted in color). **(D)** Exposure to a 10 s-long air puff during R5 activation at 1 Hz
1031 increased the mean velocity of rested flies in 5x65 mm tubes (+ retinal, *n*=10, Wilcoxon
1032 matched-pairs signed rank test). **(E)** Average locomotion during activation of R5 neurons at
1033 different frequencies. Curve: mean ± SEM. Activation of R5 neurons in rested flies at 0.1 Hz
1034 did not affect locomotion, whereas 10 Hz stimulation reduced distance travelled during and
1035 after activation (*n*=9-12 each group, Friedman tests with Dunn's multiple comparisons). **(F)**
1036 Raster plots of six example flies (58H05-GAL4>UAS-CsChrimson) before, during and after R5
1037 activation at 1 Hz (left) or 10 Hz (right). Colors indicate five designated behaviors: walking,
1038 grooming, resting (flies are immobile), loss of posture (flies are immobile and upright body
1039 posture is lost) and recovering (flies are recovering locomotion and upright body posture). **(G)**
1040 Fraction of flies that lost postural control during R5 activation at different frequencies (black).
1041 The *n* of flies for each condition is indicated in the bar plots.
1042
1043

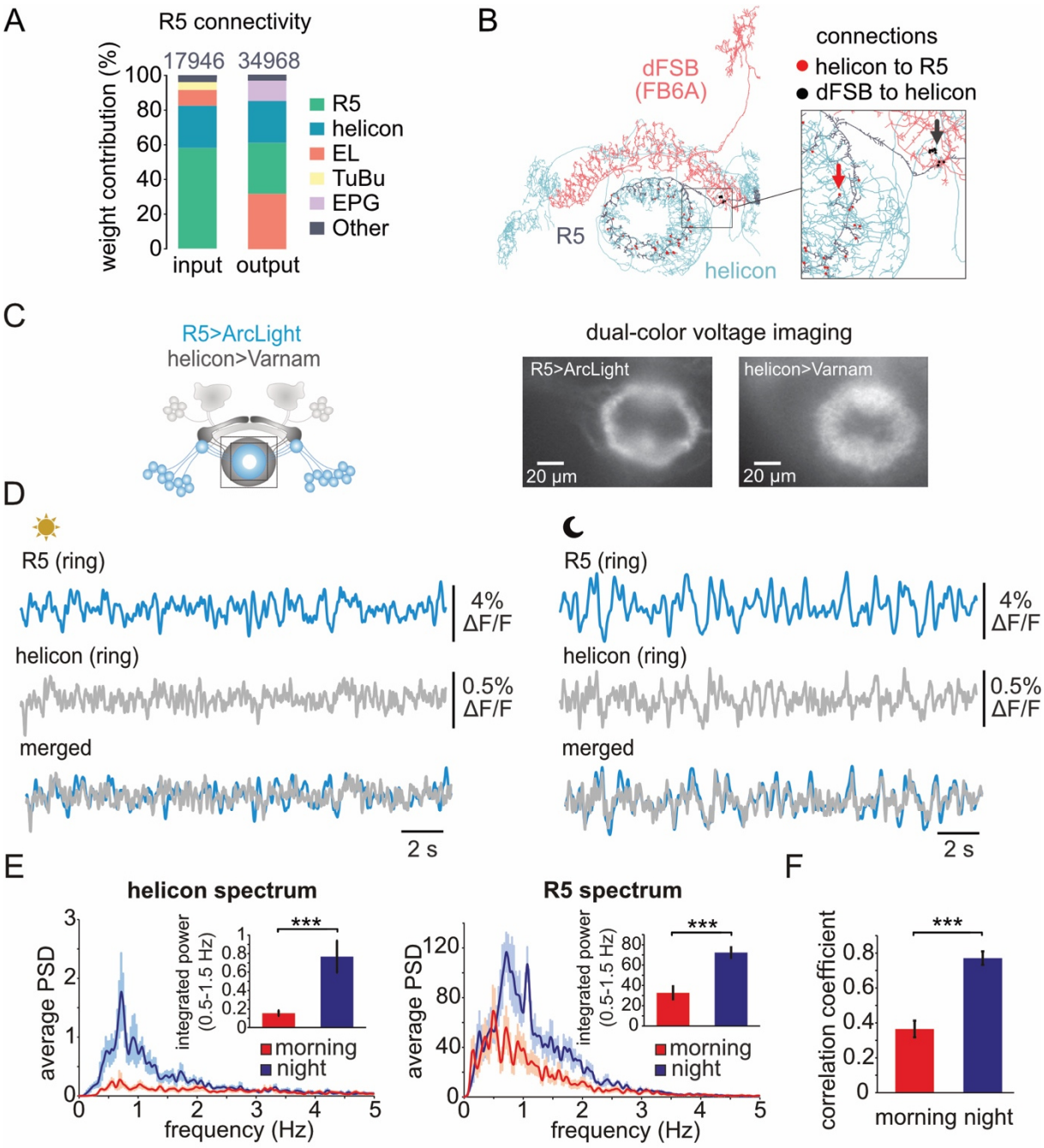

Figure 4. Sleep drive mediating and arousal gating networks synchronize electrical slow-wave patterns at night

(A) Synaptic input and output connections from R5 neurons show high connectivity with helicon cells. **(B)** Example circuit between a R5 neuron (body ID: 1200049187), helicon cell (body ID: 918334668) and dFSB neuron (neuron type FB6A) (body ID: 422191200). Red dots/arrow indicate areas of synaptic connections from the helicon cell to the R5 neuron and black dots/arrow areas of synaptic connections from the dFSB neuron to the helicon cell. **(C)** Schematic and wide-field image of presynaptic ring structures expressing the green voltage indicator ArcLight in R5 neurons (88F06-GAL4) and the red voltage indicator Varnam in helicon cells (24B11-LexA). Square indicates recording site. **(D)** Example recordings of R5 and helicon presynaptic electrical patterns recorded in the morning (ZT 2-4) and at night (ZT 14-16). **(E)** Average power spectra of compound oscillations in R5 neurons and helicon cells demonstrate

that slow-wave power (0.5-1.5 Hz) is increased at night in both networks (*n*=9-11 for helicon cells and R5 neurons, Mann-Whitney test). **(F)** Correlation between electrical patterns of helicon and R5 networks is significantly increased at night compared to the subjective morning (*n*=9-11, Mann-Whitney test).

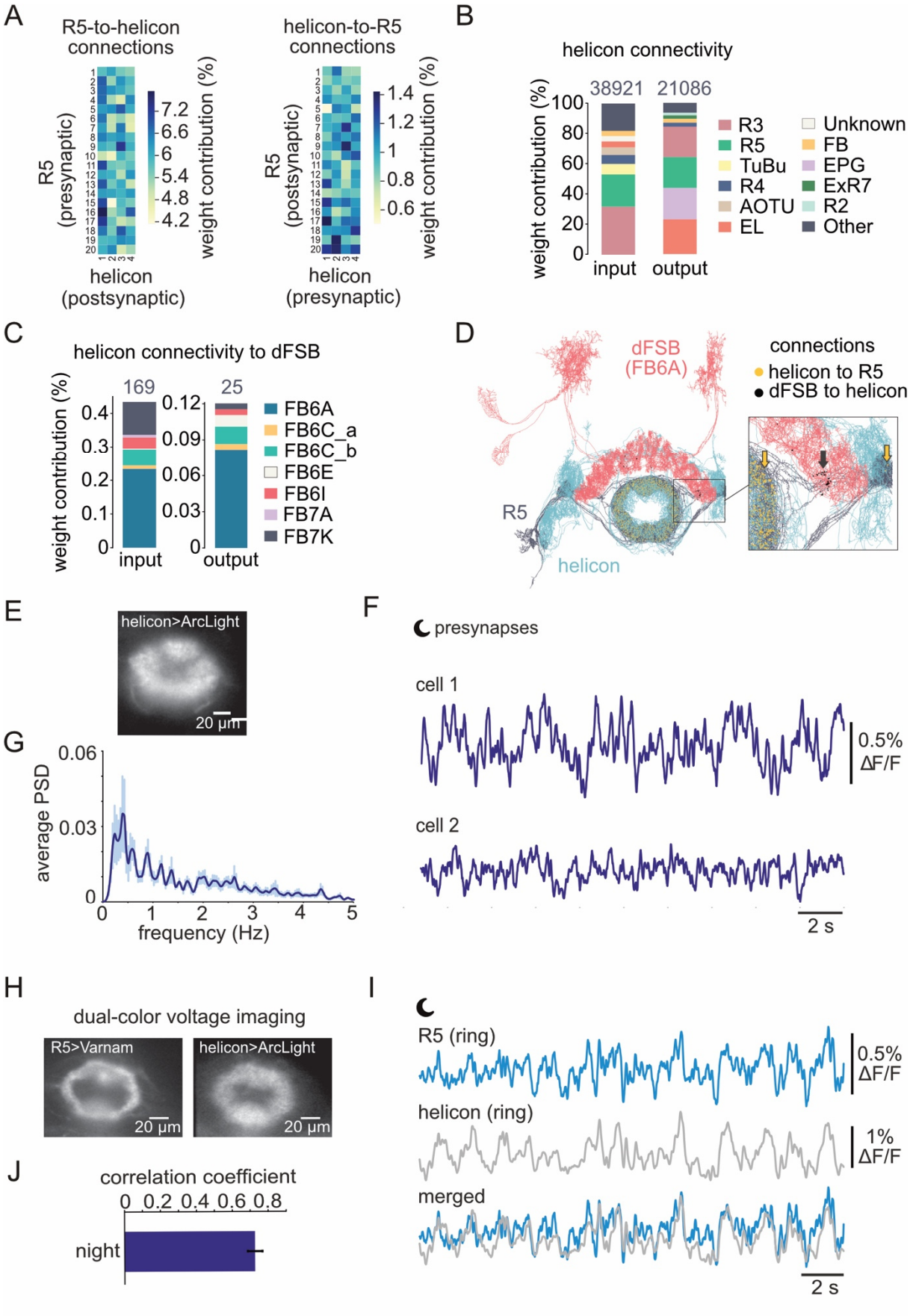
A
R5-to-helicon connections
R5 (presynaptic)
helicon (postsynaptic)
weight contribution (%)
7.2
6.6
6
5.4
4.8
4.2
helicon-to-R5 connections
R5 (postsynaptic)
helicon (presynaptic)
weight contribution (%)
1.4
1.2
1
0.8
0.6
B
helicon connectivity
weight contribution (%)
38921
21086
input
output
R3
R5
TuBu
R4
AOTU
EL
Unknown
FB
EPG
ExR7
R2
Other
C
helicon connectivity to dFSB
weight contribution (%)
169
25
input
output
FB6A
FB6C_a
FB6C_b
FB6E
FB6I
FB7A
FB7K
D
dFSB (FB6A)
connections
helicon to R5
dFSB to helicon
R5
helicon
E
helicon>ArcLight
20 µm
F
presynapses
cell 1
0.5% ΔF/F
cell 2
2 s
G
average PSD
frequency (Hz)
H
dual-color voltage imaging
R5>Varnam
helicon>ArcLight
20 µm
20 µm
I
R5 (ring)
0.5% ΔF/F
helicon (ring)
1% ΔF/F
merged
2 s
J
correlation coefficient
night

1065 **Figure S4.**
1066 **(A)** Neuron-to-neuron connectivity plot for connections from R5 to helicon (left) and vice versa
1067 (right). Number of connections were normalized to the total number of output connections of
1068 each R5 neuron (left) and to the total number of output connections of each helicon cell
1069 (right). **(B)** Top synaptic input and output connections of all helicon cells. Number of input and
1070 output connections of helicon per neuronal type were normalized to the total number of input
1071 and output connections of helicon cells. **(C)** Fraction of helicon cell input and output from dFSB
1072 neuron types normalized to the total number of input and output connections of helicon cells.
1073 **(D)** Morphological rendering of R5 neurons, helicon cell and FB6A (dFSB neuron type) neurons.
1074 Yellow dots/arrow indicate areas of synaptic connections of helicon cells to R5 neurons and
1075 black dots/arrow indicate areas of synaptic connections from the dFSB to helicon. **(E)** Wide-
1076 field image of presynapses expressing the green voltage indicator ArcLight in helicon cells
1077 (24B11-GAL4). **(F)** Example recordings of helicon presynaptic electrical patterns recorded at
1078 night (ZT 14-16). **(G)** Average power spectrum of electrical compound presynaptic activity
1079 recorded at night (n=6, ZT 14-16). **(H)** Wide-field images of presynaptic structures expressing
1080 the green voltage indicator ArcLight in helicon cells (24B11-GAL4) and the red voltage
1081 indicator Varnam in R5 neurons (58H05-LexA). **(I)** Example recordings of R5 and helicon
1082 presynaptic electrical patterns recorded at night (ZT 14-16). **(J)** Correlation between electrical
1083 patterns of helicon and R5 at night (n=8).
1084

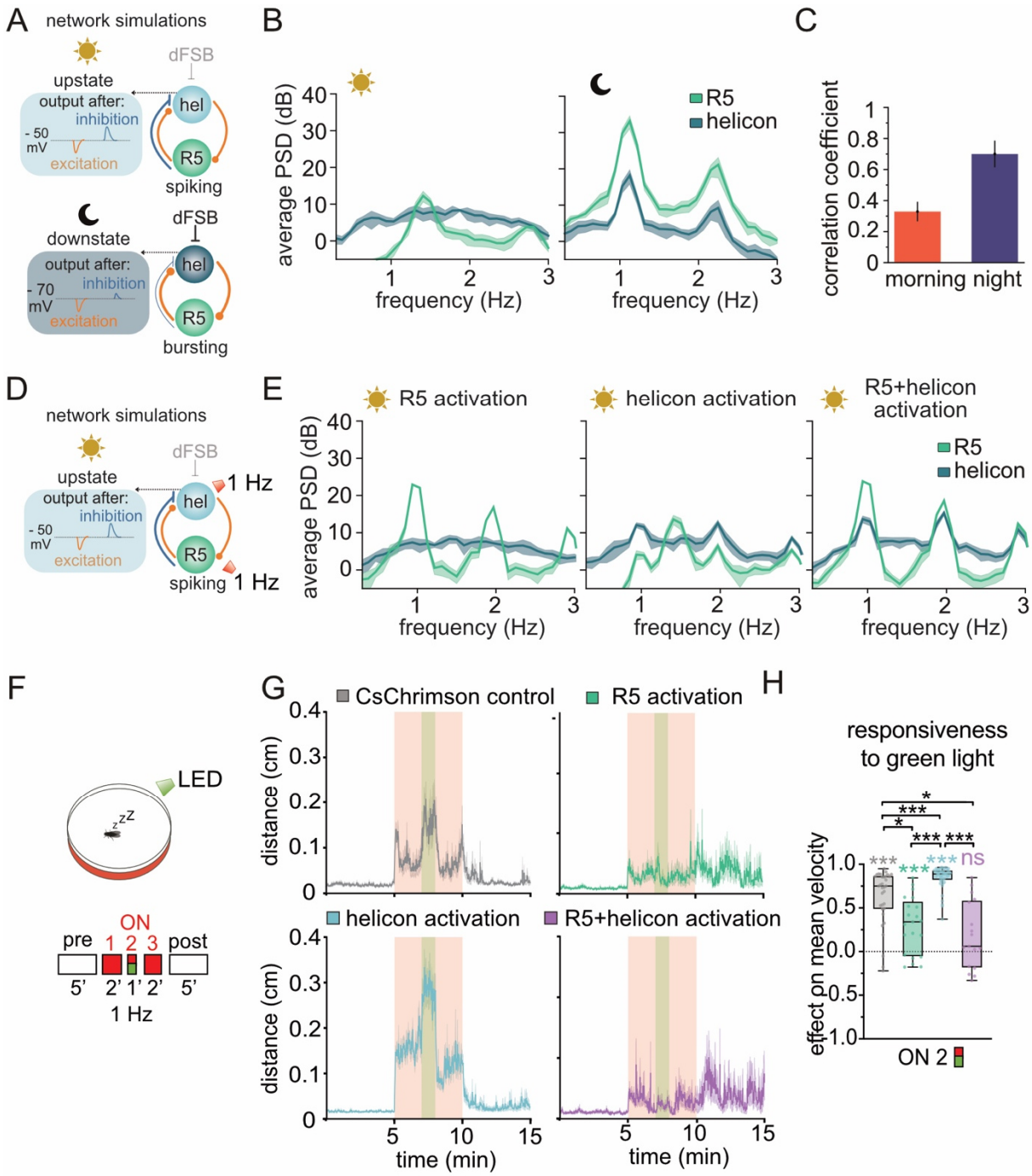

Figure 5. R5 entrains coherent oscillations in helicon to regulate behavioral responsiveness. (A) Schematic overview of simulated R5 and helicon interactions in the morning (top) and night (bottom). In our model, the helicon network is purely excitatory while R5 is mixed inhibitory and excitatory (see Fig. S5-1). In the morning configuration, R5 neurons spike and helicon cells are in a depolarized state ('upstate'). In the night configuration, R5 neurons burst, and due to inhibition mediated by the dFSB helicon cells are hyperpolarized ('downstate'). Please see Fig. S5-1 and Supplemental Experimental Procedures for more detailed information. **(B)** Simulation of R5 and helicon synchronization during the day and during the night. R5 was coupled to helicon to assess levels of synchronization within and between networks. Power spectral density (PSD) of the R5 and helicon networks in the morning and at night. In the morning, R5 did not entrain helicon activity. At night, R5 neurons became highly

synchronized and entrained helicon activity to a 1 Hz rhythm, which further promoted R5 synchronization (n=10 simulations each). **(C)** Simulated correlation coefficients of compound R5 and helicon activity in the morning and at night. Similar to the experimental data (**Fig. 4F**), correlation of the compound activity is increased at night (n=10 simulations each). **(D)** To predict the outcome of network interactions, R5 and helicon were individually and simultaneously stimulated with 1 Hz in the morning configuration. **(E)** Average PSD of R5 and helicon networks during 1 Hz stimulation in the morning configuration. 1 Hz R5 stimulation led to R5 synchronization and no helicon entrainment. 1 Hz stimulation of the helicon network led to a slight entrainment of helicon to a 1 Hz rhythm and no R5 synchronization. Simultaneous stimulation of R5 and helicon at 1 Hz led to strong R5 synchronization and helicon entrainment (n=10 simulations). **(F)** Schematic overview of optogenetic activation protocol testing behavioral responsiveness in sleeping flies. After 5 min of immobility, sleeping flies were presented with 5 min of red light at 1 Hz and a continuous green light during the stimulation. **(G)** Average locomotion traces of CsChrimson control (+ retinal, *n=33*), 58H05-LexA>LexAop-CsChrimson (R5; + retinal, *n*=22), 24B11-LexA>LexAop-CsChrimson (helicon, + retinal, *n=47*) and 58H05-LexA; 24B11-LexA>LexAop-CsChrimson flies (R5 + helicon; + retinal, *n=17)*. Curves: mean ± SEM. **(H)** Behavioral responsiveness to green light during optogenetic activation (colored asterisks indicate significance compared to baseline locomotion). Behavioral responsiveness during R5 activation was reduced compared to helicon stimulation and control. Simultaneous activation of R5 of helicon led to the strongest impairment in behavioral responsiveness, *n*=17-47 each group, Kruskal-Wallis test with Dunn's multiple comparisons (black asterisks). Behavioral data was taken during the subjective day of the flies (ZT 1-7) after a 12-19 h of sleep deprivation.

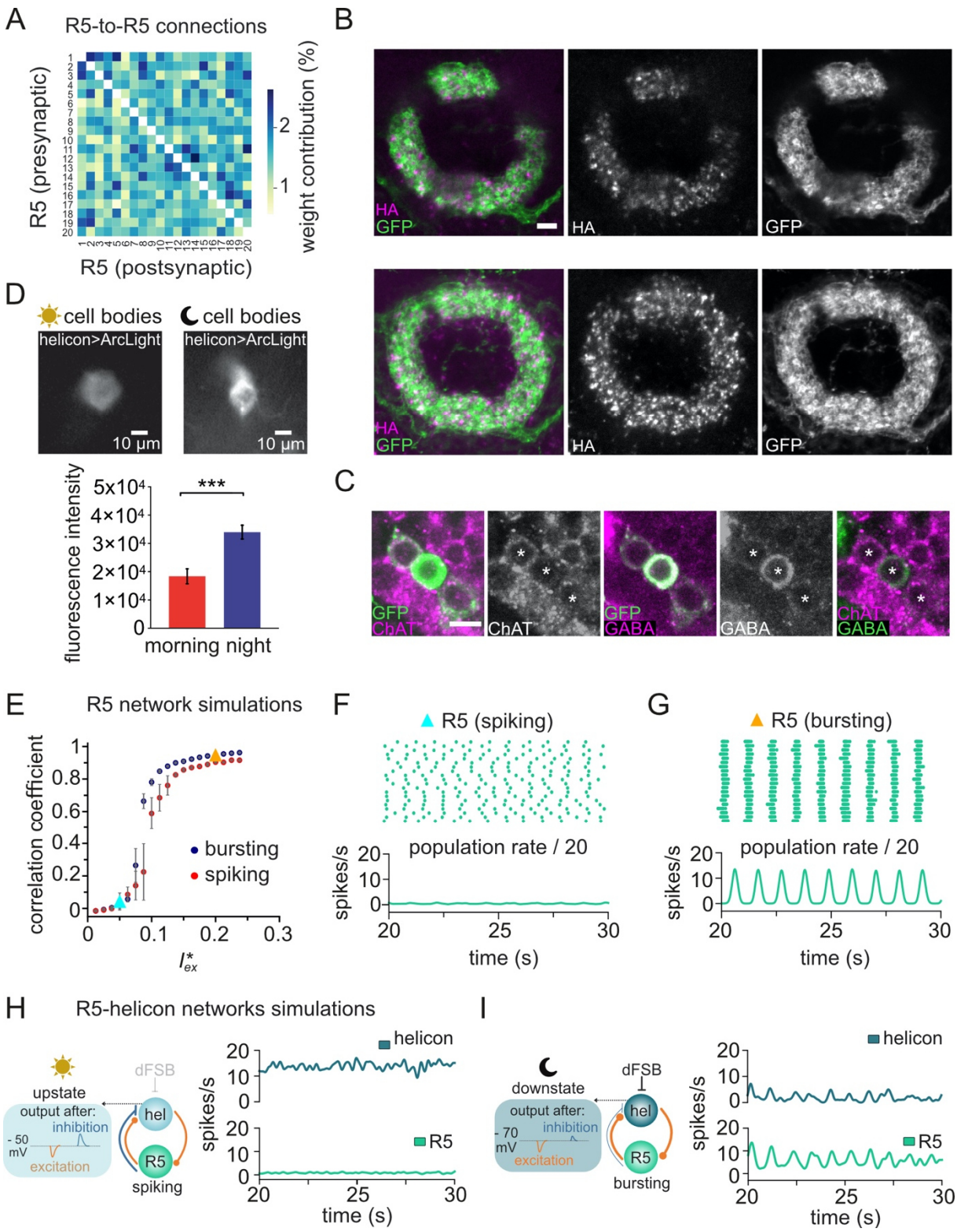

Figure S5-1

(A) Neuron-to-neuron connectivity plot for connections from R5 to R5. Number of connections were normalized to the total number of output connections of each R5 neuron. White squares indicate no direct connections. **(B)** Upper row: expression of vACht::HA and mCD8::GFP in presynaptic sites of R5 neurons targeted by 58H05-GAL4 and immunostained with anti-GFP and anti-HA. Single confocal plane. Bottom row: Maximum projection of R5 presynaptic region. Scale bar: 5 µm. **(C)** Single confocal sections of R5 cell bodies expressing mCD8::GFP under control of 58H05-GAL4 labeled with antibodies against ChAT and GABA. Images are

representative examples of one brain from four independent experiments. Asterisks indicate GFP expressing R5 neurons. Scale bar: 5 µm. **(D)** Top: wide-field images of single helicon cell bodies expressing ArcLight (24B11-Gal4) in the morning (ZT1-4) and at night (ZT12-16). Average fluorescence intensity is increased at night, indicating that helicon cells are more hyperpolarized at night relative to the morning (*n*=12, Mann-Whitney test). **(E)-(I)** Numerical simulations of R5 and helicon networks; for details on the implementation, see Supplemental Experimental Procedures. **(E)** Simulated synchronization in an isolated R5 network model. Mean correlation coefficients of 20 recurrently connected R5 neurons (spiking or bursting) for a fixed inhibitory coupling strength (-0.01) and varying excitatory coupling strength I_{exc}^{*} . Network synchronization correlated with strength of excitation, suggesting that the interaction of R5 neurons has some excitatory component and/or that other connecting networks provide excitation. Colored triangles indicate the mean correlation coefficients used in **F** and **G** (n=10 simulations each). **(F)** Top: spike raster plot of 20 R5 neurons in spiking mode and in a rather desynchronized state (I_{exc}^{*} = 0.05, mean correlation coefficient of ~ 0.3). Bottom: population rate divided by the number of neurons (n=10 simulations). **(G)** Top: spike raster plot of 20 R5 neurons in burst-firing mode and in a highly synchronized state (I_{exc}^{*} = 0.20, mean correlation coefficient of ~0.9). Bottom: population rate divided by the number of neurons (n=10 simulations). **(H)** Left: schematic summary of simulated R5 and helicon interactions in the morning (see Fig. 5A). Right: compound activity of helicon and R5 neurons in the morning normalized by the number of neurons in each network. In the morning, SWA was weak in both networks (n=10 simulations). **(I)** Left: schematic summary of simulated R5 and helicon interactions at night (see Fig. 5A). Right: compound activity of membrane potential dynamics of helicon cells and R5 neurons at night (see Fig. 5A) normalized by the number of neurons in each network. In the evening, both networks showed increased SWA activity (n=10 simulations).

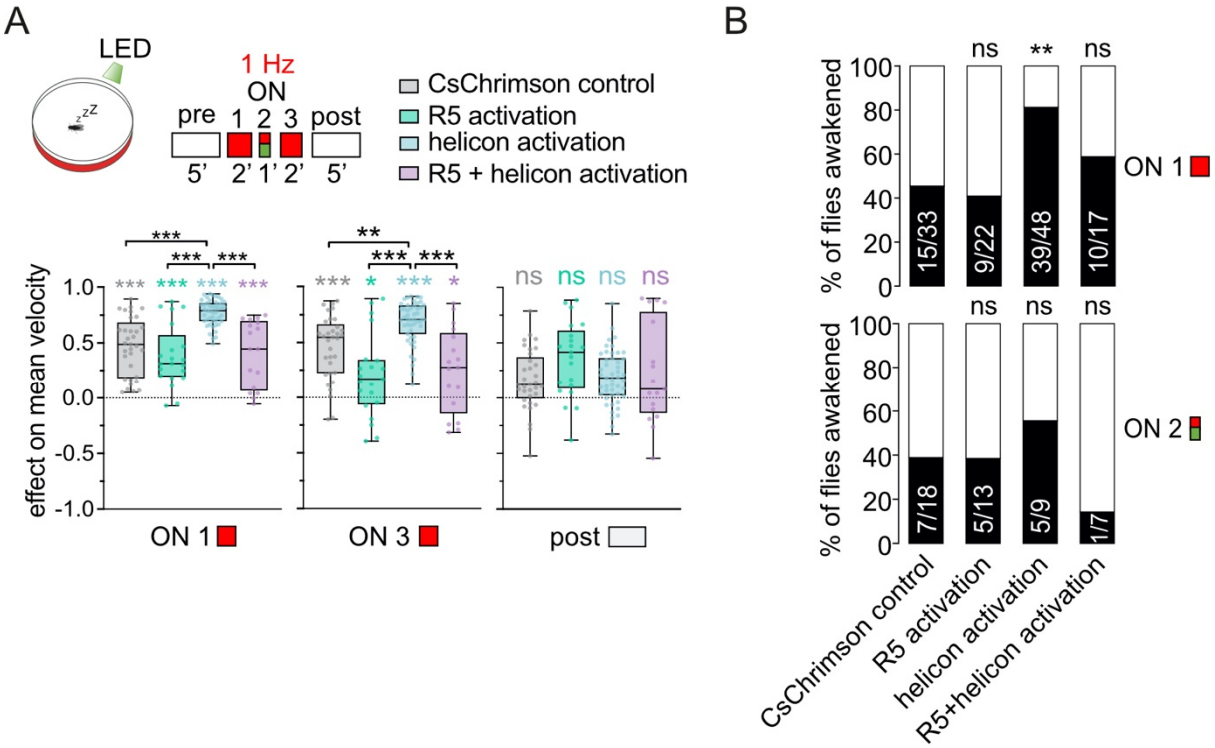

Figure S5-2

(A) Top: schematic overview of optogenetic activation protocol to test behavioral responsiveness during network activation in sleep deprived flies (described in Fig. 5F). Bottom: effect of optogenetic stimulation at different times of the experiment. The effect of helicon activation on locomotion differed to that of R5 and R5+helicon activation, *n=33* for CsChrimson control, *n*=22 for 58H05-LexA>LexAop-CsChrimson, *n*=47 for 24B11-LexA>LexAop-CsChrimson and *n*=17 for 58H05-LexA;24B11-LexA>LexAop-CsChrimson, Kruskal-Wallis test with Dunn's multiple comparisons (comparisons between genotypes, black asterisks) and Wilcoxon signed-rank tests (comparisons to baseline locomotion, colored asterisks). Behavioral data was acquired during the subjective day of the flies (ZT 1-7) after 12-19 h of sleep deprivation. **(B)** Percentage of sleeping flies that started walking ('awakened') at the beginning of the optogenetic stimulation (top, 'ON 1') or when exposed to green light (bottom, 'ON 2'). 1 Hz stimulation of the helicon network led to more flies waking up at the beginning of the stimulation when compared to the genetic control, Binomial test. The *n* of flies for each condition is indicated in the bar plots.

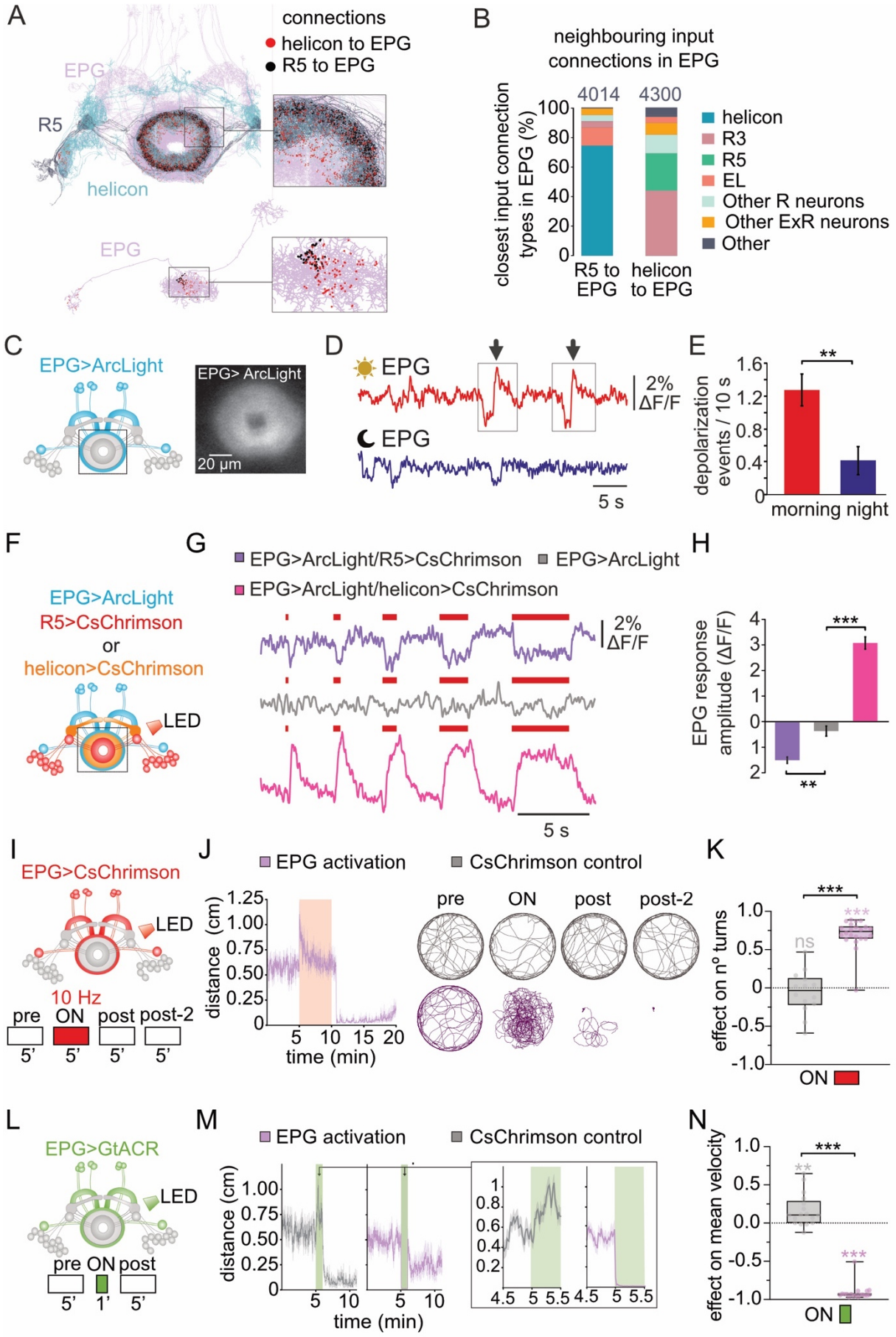
A
connections
helicon to EPG
R5 to EPG
EPG
R5
helicon
EPG
B
neighbouring input connections in EPG
closest input connection types in EPG (%)
4014
4300
R5 to EPG
helicon to EPG
helicon
R3
R5
EL
Other R neurons
Other ExR neurons
Other
C
EPG>ArcLight
EPG> ArcLight
20 µm
D
EPG
EPG
2% ΔF/F
5 s
E
depolarization events / 10 s
morning
night
F
EPG>ArcLight
R5>CsChrimson
or
helicon>CsChrimson
LED
G
EPG>ArcLight/R5>CsChrimson
EPG>ArcLight
EPG>ArcLight/helicon>CsChrimson
2% ΔF/F
5 s
H
EPG response amplitude (ΔF/F)
I
EPG>CsChrimson
LED
10 Hz
pre
ON
post
post-2
5'
5'
5'
5'
J
EPG activation
CsChrimson control
distance (cm)
time (min)
pre
ON
post
post-2
K
effect on nº turns
ns
ON
L
EPG>GtACR
LED
pre
ON
post
5'
1'
5'
M
EPG activation
CsChrimson control
distance (cm)
time (min)
N
effect on mean velocity
ON

1176 **Figure 6: R5 and helicon regulate behavioral responsiveness via antagonistic inputs to the**
1177 **navigational system.**
1178 **(A)** Top: the helicon-R5-EPG circuitries are strongly interconnected at the level of the ring.
1179 Morphological renderings of R5 neurons, helicon cells and EPG neurons. Red dots depict
1180 synaptic connections of helicon cells to EPG neurons and black dots show synaptic connections
1181 of R5 to EPG. Bottom: Location of R5 and helicon synapses projecting to a single EPG neuron
1182 (bodyId: 387364605). **(B)** At the level of EPG neuron dendrites, synaptic input connections
1183 from R5 neurons (R5-to-EPG) are found in proximity to input connections from helicon cells
1184 (helicon-to-EPG). Similarly, helicon-to-EPG synaptic connections are found in proximity to R5-
1185 to-EPG connections and other ring neurons-to-EPG connections. Bar plots indicate the fraction
1186 of closest synaptic connections for R5-to-EPG and helicon-to-EPG per neuron type. The
1187 numbers of R5-to-EPG and helicon-to-EPG synaptic connections analyzed are indicated. **(C)**
1188 Schematic overview and wide-field image of EPG neurons expressing the voltage indicator
1189 ArcLight (60D05-GAL4). **(D)** Example recordings of EPG electrical patterns recorded in the
1190 morning (ZT 2-4) and at night (ZT 14-16) indicating reduced activity at night. Squares indicate
1191 spontaneous non-oscillatory events during the day. **(E)** Incidence of depolarization events is
1192 markedly reduced at night (*n*=12, Mann-Whitney test). **(F)** Schematic overview of EPG
1193 recording site (60D05-GAL4) during optogenetic activation of R5 (58H05-LexA) and helicon
1194 (24B11-LexA). **(G)** Example recordings showing that activation of R5 neurons leads to net
1195 hyperpolarization of the EPG network and that helicon cells depolarize it. To suppress
1196 spontaneous activity during helicon activation we used a high Mg^{2+} solution. **(H)** EPG response
1197 amplitudes during optogenetic activation reveals that R5 mediates hyperpolarization while
1198 helicon mediates depolarizations, n=25-30 stimulations in 5-6 independent brains, Kruskal-
1199 Wallis with posthoc Dunn's test. **(I)** Schematic overview of the optogenetic protocol (as
1200 described in Fig. 3C) used to activate EPG neurons under control of 60D05-GAL4. **(J)** Left:
1201 average locomotion traces of 60D05-GAL4>UAS-CsChrimson and control flies (+ retinal, *n*=22).
1202 Right: example trajectories. **(K)** Optogenetic activation of EPG at 10 Hz increased number of
1203 turns, *n*=14-22 each group, Mann-Whitney test (comparisons between genotypes, black
1204 asterisks) and Wilcoxon signed-rank test (comparisons to baseline locomotion, colored
1205 asterisks). **(L)** Schematic overview of the optogenetic protocol used to hyperpolarize EPG
1206 neurons expressing UAS-GtACR1 under the control of 60D05-GAL4. After 5 min of baseline
1207 activity, flies are exposed to 1-min continuous green light from below and allowed to recover
1208 for 5 min. **(M)** Average locomotion traces of GtACR1 control (+ retinal, *n*=17) and 60D05-
1209 GAL4>UAS-GtACR1 flies (+ retinal, *n*=18). Curves: mean ± SEM. **(N)** Constant inactivation of
1210 EPG neurons drastically reduced mean velocity in 60D05-GAL4>UAS-GtACR1 flies compared
1211 to control flies, *n*=17-18 for each group, Mann-Whitney test (comparisons between
1212 genotypes, black asterisks) and Wilcoxon signed-rank test (comparisons to baseline
1213 locomotion, colored asterisks).

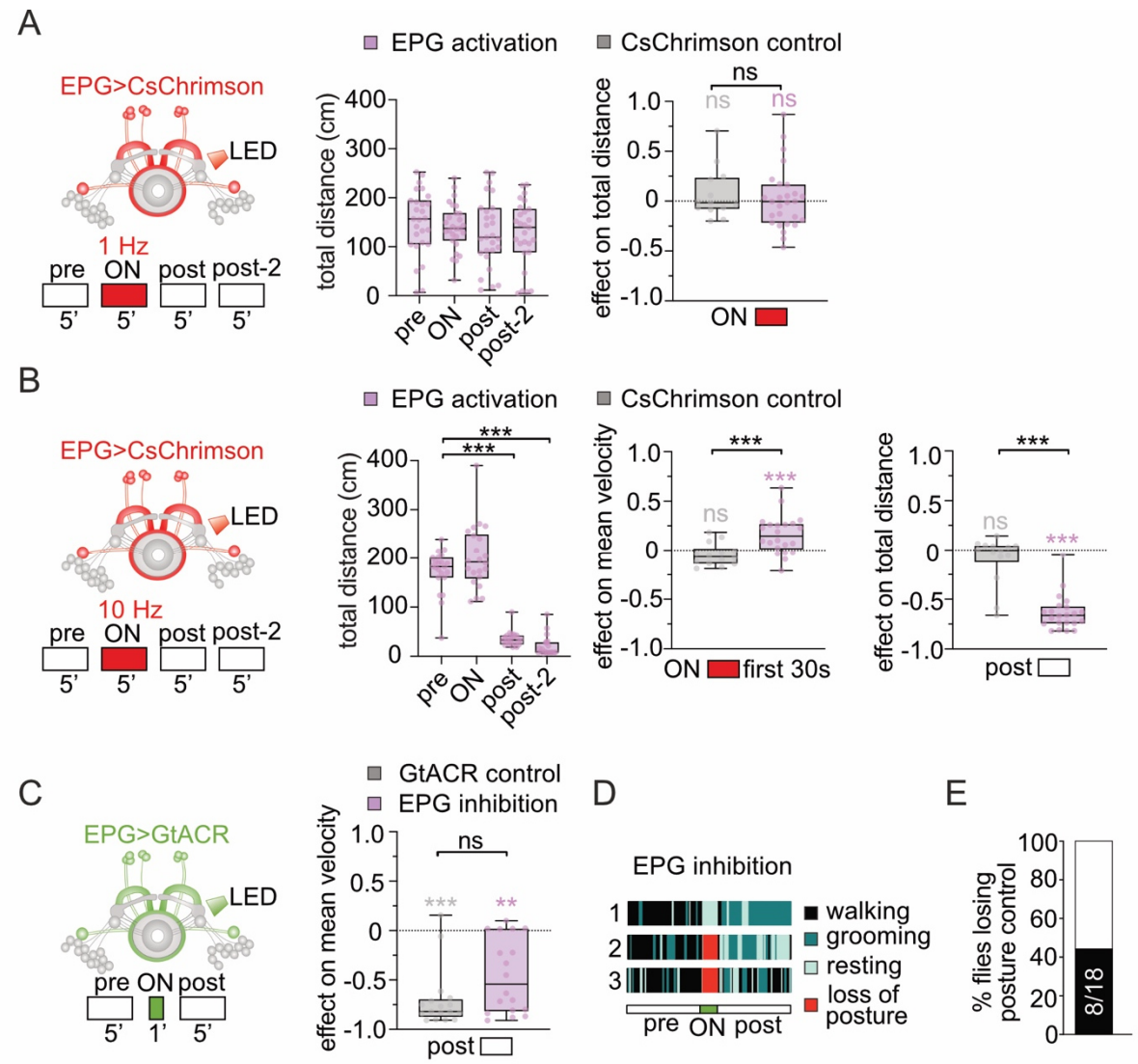

Figure S6.

(A) Schematic overview of the optogenetic protocol used to activate EPG neurons at 1 Hz for the 60D05-GAL4 control using the stimulation protocol described in Fig. 3C. Activation of EPG neurons in rested flies at 1 Hz did not affect locomotion (*n*=27, Friedman test with Dunn's multiple comparisons). The effect on distance travelled of 1 Hz stimulation in 60D05-GAL4>UAS-CsChrimson flies (+ retinal) did not differ from that of control flies (+ retinal), *n*=13-27 each group, Mann-Whitney test (comparisons between genotypes depicted in black) and Wilcoxon signed-rank test (comparisons to baseline locomotion depicted in color). **(B)** Schematic overview of 10 Hz EPG activation under 60D05-GAL4 control in rested flies. High frequency activation of EPG neurons reduced locomotion after stimulation, (*n*=22, Friedman test with Dunn's multiple comparisons). 10 Hz EPG activation led to an increased mean velocity in the first seconds of stimulation and decreased distance travelled after stimulation compared to control flies, *n*=14-22 each group, Mann-Whitney test (comparisons between genotypes depicted in black) and Wilcoxon signed-rank test (comparisons to baseline locomotion depicted in color). **(C)** Schematic of constant inactivation of EPG neurons expressing UAS-GtACR1. EPG block did not affect mean velocity after optogenetic inhibition, *n*=17 for GtACR1 control and *n*=19 for EPG inhibition, Mann-Whitney test (comparisons between genotypes depited in black) and Wilcoxon signed-rank test (comparisons to baseline locomotion depicted in color). **(D)** Raster plots of three example flies (60D05-GAL4>UAS-

1234 CsChrimson) before, during and after EPG inhibition. Colors indicate four designated
1235 behaviors: walking, grooming, resting (flies are immobile) and loss of posture (flies are
1236 immobile and upright body posture is lost). **(G)** Fraction of 60D05-GAL4>UAS-CsChrimson flies
1237 that lost postural control during EPG inhibition (black). The *n* of flies is indicated in the bar
1238 plot.
1239

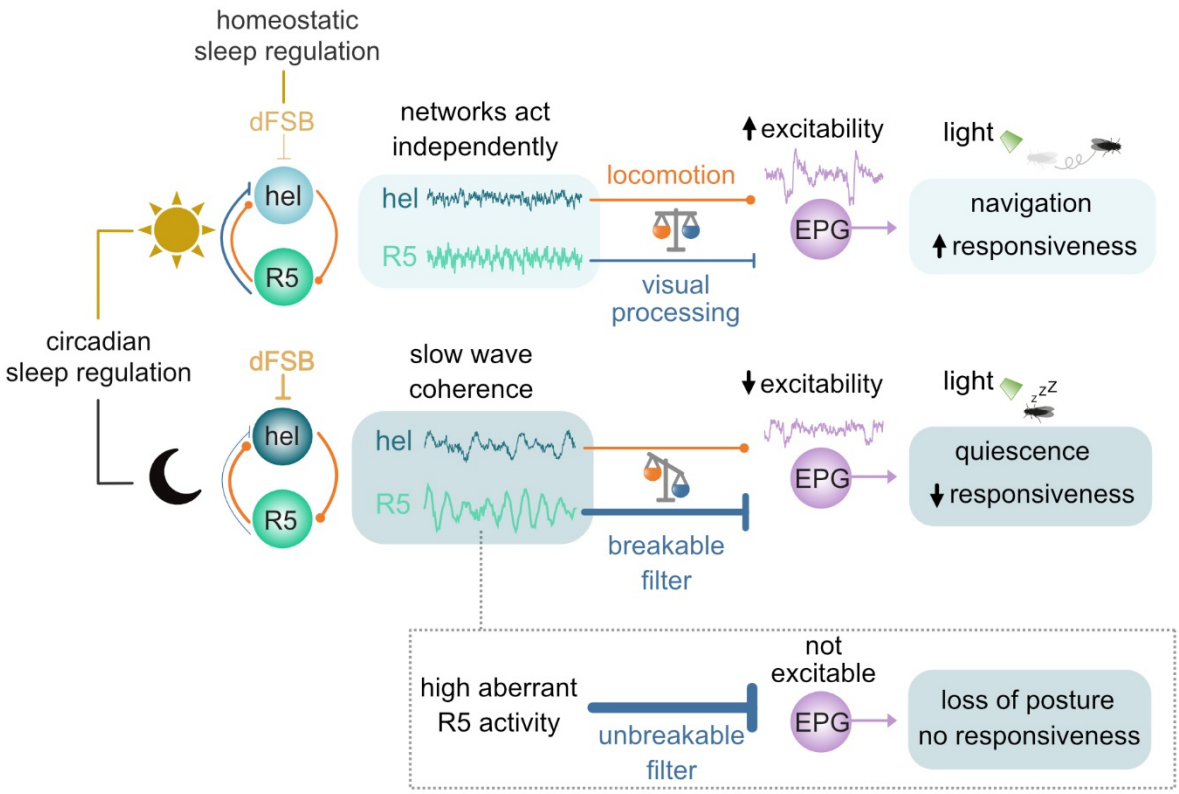

Figure 7: Diurnal modulations of network interactions generate coherent slow-wave activity that act as neural filters to promote quiescence

Daytime: Due to reduced activity of the fly's sleep homeostat (dFSB), R5 does not entrain slow-wave activity in helicon (hel). High frequency output from helicon gates locomotion via excitation (orange line) of head-direction neurons (EPG), which promotes navigation and increases responsiveness to visual stimuli. **Nighttime:** Increased activity of the dFSB and circadian regulation hyperpolarize helicon and drive entrainment of slow-wave coherence through R5. Network coherence and the temporal structure of inhibitory input provided by R5 reduce excitability of EPG neurons, creating a breakable neural filter, which promotes quiescence and reduces behavioral responsiveness. Aberrant high inhibition of EPG by R5 leads to loss of posture and induces a coma-like reversible state of complete unresponsiveness.